GPM/DPR Level-2
Algorithm Theoretical Basis Document

Authors: Toshio Iguchi, Shinta Seto, Robert Meneghini,
Naofumi Yoshida, Jun Awaka, Minda Le,
V. Chandrasekar, and Takuji Kubota

December 2010
Revised October 2014
Revised January 2015
Revised April 2015
Revised August 2015
Revised February 2016
Revised March 2016
Revised April 2017 for V05

TABLE OF CONTENTS

0. INTRODUCTION AND CAVEATS

This document describes the basic idea of DPR data processing. It was originally written for the algorithm used in the at-launch version (V3). The algorithm has been modified and improved since then. Although the basic idea of data processing remains the same, the actual flow of processing, in particular that in the solver module, has changed substantially. As a result, some part of description in section 3.1 may not be relevant any more.

Major changes in the DPR algorithm from V4 to V5 are summarized here.

In level 1 algorithm, based on the new calibration results, the system parameters of DPR were re-examined, and the offset parameters for the transmitting powers, receiver's gains, the beam widths, and the pulse width of both KuPR and KaPR were redefined. As a result, Z_m of KuPR has increased by about +1.3 dB, and Z_m of KaPR by about +1.2 dB.

In level 2 algorithm, in addition to the changes in the DPR L1 calibration, adjustment factors were introduced in the preparation module to remove small trends in the overall system gains in KuPR and KaPR. The adjustment factors change the measured received powers only by a small fraction of dB. New flags, such `flagHeavyIcePrecip`, `flagSurfaceSnowfall`, `flagAnvil` and `snowIceCover`, are introduced in V5. A DSD database that depends on the month, region, surface type and rain type was created from the statistics of DSD parameters estimated with the dual-frequency algorithm and is applied to the single frequency (Ku-only and Ka-only) data processing. These changes are described in the relevant sections of this document.

1. OBJECTIVES

The objective of the level 2 DPR algorithms is to generate from the level 1 DPR products radar-only derived meteorological quantities on an instantaneous FOV (field of view) basis. A subset of the results will be used by the level 2 combined radar-radiometer algorithm and the level 3 combined and radar-only products.

The general idea behind the algorithms is to determine general characteristics of the precipitation, correct for attenuation and estimate profiles of the precipitation water content, rainfall rate and, when dual-wavelength data are available, information on the particle size distributions in rain and snow. It is particularly important that dual-wavelength data will provide better estimates of rainfall and snowfall rates than the TRMM PR data by using the particle size information and the capability of estimating, even in convective storms, the height at which the precipitation transitions from solid to liquid.

2. BACKGROUND INFORMATION

2.1 Historical Perspective

The Dual-Frequency Precipitation Radar (DPR) on the GPM core satellite will be the second space-borne precipitation radar, following the first such radar, the Precipitation Radar (PR), launched on the TRMM satellite in November, 1997. The TRMM PR has already revolutionized the measurement of precipitation from space by providing high resolution 3-dimensional rain echoes in the tropics and subtropics. The DPR consists of Ku-band (13.6GHz) and Ka-band (35.5GHz) channels. A major source of error in the rainfall estimates from the TRMM/PR comes from the uncertainty in the conversion of radar reflectivity into rainfall rate. This uncertainty originates in the variations of the raindrop size distribution (DSD) that changes by region, season and rain type. One of the reasons for adding the Ka-band frequency channel to the DPR is to provide information on the DSD that can be obtained from non-Rayleigh scattering effects at the higher frequency.

Another reason for the new Ka-band channel is to provide more accurate estimates of the phase-transition height in precipitating systems. This information is very important not only in increasing the accuracy of rain rate estimation by the DPR itself, but in improving rain estimation by passive microwave radiometers.

The third reason for the Ka-band channel arises from the fact that the GPM core satellite will provide coverage up to about 65 degrees latitude; by increasing the sensitivity of this channel, a larger fraction of snow events will be detected.

Since the Ku-band channel of the DPR is very similar to the TRMM PR, the principal challenge in the development of the DPR level 2 algorithms is to combine the new Ka-band data with the Ku-band data to achieve the objectives mentioned above.

2.2 Instrument Characteristics

The DPR consists of the Ku-band precipitation radar and the Ka-band precipitation radar. They are abbreviated as KuPR and KaPR, respectively. These Earth-pointing KuPR and KaPR instruments will provide rain sensing over both land and ocean, both day and night. The KuPR and KaPR design specifications, with all active phased array elements functioning, are shown in Table 2.2-1. The spacecraft orbital information is shown in Table 2.2-2.

Figure 2.2-1 shows the DPR scan pattern. KuPR's scan pattern is similar to that of the TRMM PR. It has 49 footprints in a scan and the footprint size is about 5 km in diameter. The scan swath is 245 km. The KaPR also has 49 footprints, but these are divided into two types of scan. In the first type of scan (Ka_MS), the beams are matched to the central 25 beams of KuPR, providing a swath of 120 km. In the second type of scan (Ka_HS), the KaPR is operated in the high-sensitivity mode to detect light rain and snow. In this case, its beams are interlaced within the scan pattern of the matched beams as shown in Fig. 2.2-1. The KuPR and

KaPR for the Ka_MS scan have the same range resolution (250 m), while the range resolution of data in Ka_HS is 500m. In both cases, radar echoes are over-sampled at twice the rate of the corresponding resolution: 125 m for the matched beams and 250 m for the Ka_HS.

Table 2.2-1 DPR Design Specification

Item	KuPR	KaPR
Swath Width	245 km	120 km
Range Resolution	250 m	250/500 m
Spatial Resolution	5.2 km (Nadir at the height of 407 km)	
Beam Width	0.71° (Center Beam)	
Transmitter	128 Solid State Amplifiers	
Peak Transmit Power[1]	1012.0 W	146.5 W
Pulse Repetition Freq.[2]	4000 to 4500 Hz	
Pulse Width	two 1.6 μs pulses	two 1.6 μs pulses (matched beams) two 3.2 μs pulses (interlaced scans)
Beam Number	49	49 (25 in matched beams and 24 in interlaced scans)
Min. measurable rain rate	0.5 mm/h	0.2 mm/h
Beam matching error	Less than 1000 m	
Observable range	19 km to Surface (to −5 km near nadir)	
Dynamic range	From −5 dB below the system noise level to +5 dB above the nominal maximum surface echo level	
Receiver power accuracy	±1 dB	
Scan Angle	±17° Cross Track	±8.5° Cross Track
Frequencies	13.597 and 13.603 GHz	35.547 and 35.553 GHz
Bandwidth	14 MHz	
Max. Mass	472 kg	336 kg
Power (max)	446 W (orbit average)	344 W (orbit average)
Science Data Rate (max)	109 kbps	81 kbps
	(The Total of KuPR and KaPR is 190 kbps)	
Housekeeping Data Rate[3]	1 kbps (nominal)	

1. This parameter is for informational purposes in the ICD.
2. In nominal operation mode.
3. 1 kbps may increase up to 2 kbps during SCDP switch-overs.

Table 2.2-2 Spacecraft Orbital Information

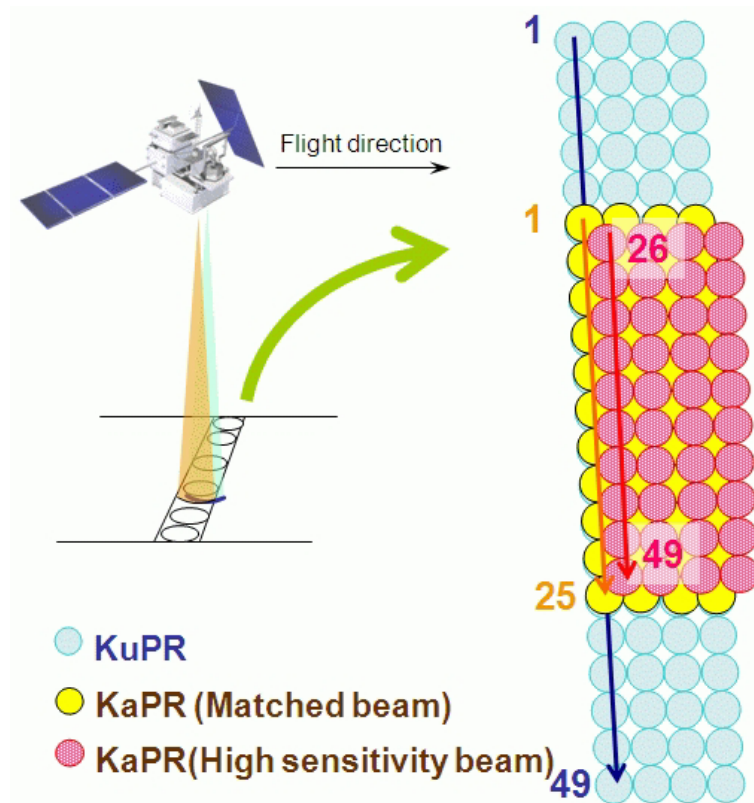| Inclination	65°
Mean semi-major axis	6776.14 km
S/C Altitude Control Box	±1 km
Orbit Eccentricity	0.00010 (0-0.0005 tolerance)
Geodetic Altitude Variation Range	397 km to 419 km

Figure 2.2-1. DPR scan pattern.

Figure 2.2-2 shows the observation range. The DPR's echo sampling is designed to cover a range that, at minimum, extends from the surface to 19 km above the sea level (or from the Ellipsoid). The pulse repetition interval is adjusted according to the satellite altitude and the angle of observation. As a result, the number of independent samples changes slightly as a function of the scan angle.
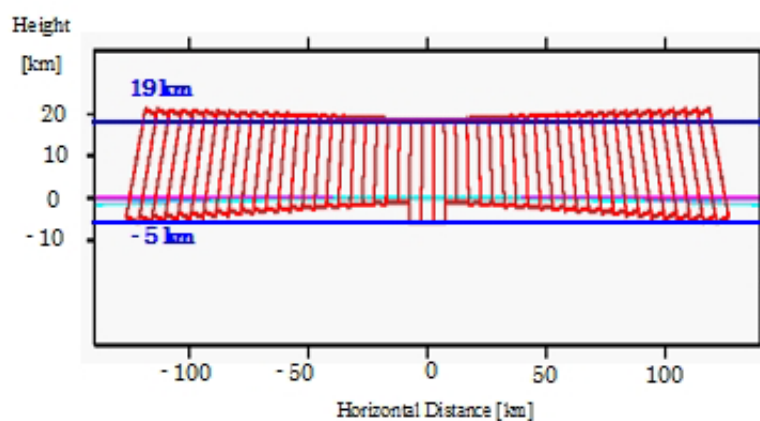

Figure 2.2-2 DPR's data sampling range

3. ALGORITHM DESCRIPTION

3.1. Theoretical Description

3.1.1. Physical Basis of the Algorithm

The radar transmits a pulse of radio waves and receives an echo from an object. The object in the case of precipitation radar is a distribution of rain drops in the volume defined by the antenna directivity, the pulse width and the time between the transmission and the reception of the pulse. The received power P_r from rain at range r is proportional to the apparent radar reflectivity factor $Z_{m0}(r)$.

$$P_r(r) = \frac{C|K|^2}{r^2} Z_{m0}(r) \qquad (3.1\text{-}1)$$

where C is the radar constant, and K is a constant defined as a function of complex refractive index m of scattering particles by the following equation.

$$K = \frac{m^2 - 1}{m^2 + 2} \qquad (3.1\text{-}2)$$

When the radar electric specifications and range r are given, Z_{m0} can be calculated from P_r. Therefore, we can assume that $Z_{m0}(r)$ can be derived from a measurement of the echo power. Z_{m0} is related to the effective radar reflectivity factor Z_e by

$$Z_{m0}(r) = A(r)Z_e(r) \qquad (3.1\text{-}3)$$

where A is the attenuation factor. The effective radar reflectivity factor Z_e can be expressed in terms of the backscattering cross section $\sigma_b(D)$ of a precipitation particle of diameter D and the particle size distribution $N(D)$:

$$Z_e = \frac{\lambda^4}{\pi^5 |K|^2} \int \sigma_b(D) N(D) \, dD \qquad (3.1\text{-}4)$$

Here λ is the wavelength of the electromagnetic waves, and rainfall rate R can also be expressed in terms of $N(D)$,

$$R = \int V(D) v(D) N(D) \, dD \qquad (3.1\text{-}5)$$

where $V(D)$ is the volume of the precipitation particle of diameter D, $v(D)$ is its falling velocity.

If $N(D)$ is characterized by a single parameter, for example D^*, then Z_e and D^* are in one-to-one correspondence. Since R and D^* is in a one-to-one correspondence as well, once Z_e is obtained, then $N(D)$ can be specified by D^* corresponding to this Z_e, and R can be calculated. In this case, therefore, the attenuation correction used to obtain Z_e from Z_{m0} is the primary problem to be solved. This is the principle of rain estimation for a single frequency radar

such as the TRMM PR. In fact, however, variations of $N(D)$ in nature cannot be characterized sufficiently by a single parameter in many cases. As a result, rain estimates from a single frequency radar often involve errors and biases.

In contrast, variations in $N(D)$ can be well represented by two parameters as far as the conversion from Z_e to R is concerned. If rain is measured by the radar at two wavelengths and if one of the wavelengths divided by 2π is smaller than or comparable to the average raindrop size, then the corresponding backscattering cross section will deviate from that of Rayleigh scattering, and Z_e at this wavelength differs from Z_e at the longer wavelength where Rayleigh scattering generally applies. This situation enables us to estimate two parameters of the model function of $N(D)$ and results in a better estimate of rainfall rate. This is the idea of rainfall estimation with a dual-wavelength radar. In other words, if $N(D)$ is characterized by two parameters N^* and D^*, Z_e at two wavelengths Z_{e1} and Z_{e2} become functions of N^* and D^*,

$$Z_{e1}(N^*, D^*) = \frac{\lambda_1^4}{\pi^5 |K|^2} \int \sigma_{b1}(D) N(D; N^*, D^*) \, dD \tag{3.1-6}$$

$$Z_{e2}(N^*, D^*) = \frac{\lambda_2^4}{\pi^5 |K|^2} \int \sigma_{b2}(D) N(D; N^*, D^*) \, dD \tag{3.1-7}$$

Once Z_{e1} and Z_{e2} are given, we can solve (3.1-6) and (3.1-7) for N^* and D^*, and R can be calculated from $N(D; N^*, D^*)$.

As in the single-wavelength case, the attenuation corrections to obtain Z_{e1} and Z_{e2} at two frequencies from measured or apparent radar reflectivity factors Z_{m1} and Z_{m2} are crucial. Since the major attenuation comes from precipitation itself, and the DSD parameters can be estimated from Z_{e1} and Z_{e2}, we look for a profile of pairs of DSD parameters (one pair per range gate) that gives the attenuation corrected profiles of Z_{e1} and Z_{e2} that are consistent with the attenuations caused by the precipitation particles whose size distributions are characterized by these DSD parameters. This part of the algorithm is the heart of the rainfall retrieval with dual-frequency radar data. Details of the algorithm are described in section 3.2.5.

Attenuation caused by non-precipitation particles and atmospheric gases must be compensated for beforehand. Specifically, we need to take into account the attenuation caused by cloud water, water vapor and oxygen molecules. Meteorological data and storm models are used to estimate their profiles for this purpose.

3.1.1-1 Effective radar reflectivity factor Z_e, specific attenuation k and measured radar reflectivity factor

The effective radar reflectivity factor Z_e is given by (3.1-4). Similarly, the specific attenuation k is given in terms of the drop size distribution $N(D)$ and the total extinction cross section $\sigma_e(D)$ by

$$k = c_k \int \sigma_e(D) N(D) \, dD \tag{3.1-8}$$

9

where $c_k = 0.01/\ln(10)$ if k is expressed in [dB (km^{-1})], $\sigma_e(D)$ in [mm^2], and $N(D)$ in [mm^{-1} m^{-3}]. Let r [km] denote the distance from the radar along the range. The measured radar reflectivity factor $Z_{m0}(r)$ [mm^6 m^{-3}] involves the attenuation by precipitation particles $A_{\mathrm{P}}(r)$ and by non-precipitation particles $A_{\mathrm{NP}}(r)$ as is expressed in the following equation.

$$Z_{m0}(r) = Z_e(r)A_{\mathrm{NP}}(r)A_{\mathrm{P}}(r) = Z_e(r)A_{\mathrm{NP}}(r)\exp\left[-0.2\ln(10)\int_0^r k(s)\,ds\right] \qquad (3.1\text{-}9)$$

where s is a dummy variable. Equation (3.1-9) can be rewritten in decibels as shown below.

$$10\log_{10} Z_{m0}(r) = 10\log_{10} Z_e(r) + 10\log_{10} A_{\mathrm{NP}}(r) - 2\int_0^r k(s)\,ds \qquad (3.1\text{-}10)$$

After attenuation correction for non-precipitation particles, $Z_{m0}(r)$ becomes $Z_m(r)$, where $Z_m(r)$ is given by.

$$Z_m(r) = Z_{m0}(r)A_{\mathrm{NP}}^{-1}(r) = Z_e(r)A_{\mathrm{P}}(r) \qquad (3.1\text{-}11)$$

By substituting Eq. (3.1-11) into Eq. (3.1-9), the following equation is obtained.

$$10\log_{10} Z_m(r) = 10\log_{10} Z_e(r) - 2\int_0^r k(s)\,ds \qquad (3.1\text{-}12)$$

3.1.1-2 HB method

Let us assume a power-law relation between k and Z_e as shown below.

$$k(r) = \alpha(r)Z_e^\beta(r) \qquad (3.1\text{-}13)$$

where α and β are coefficients, α can be range dependent, but β should be constant along the range. With the help of Eq. (3.1-13), Eq. (3.1-12) can be solved for Z_e and written in the form of (3.1-14),

$$Z_e(r) = \frac{Z_m(r)}{\left[1 - 0.2\ln(10)\beta\int_0^r \alpha(s)Z_m^\beta(s)\,ds\right]^{1/\beta}} \qquad (3.1\text{-}14)$$

Alternatively, the equation can be solved for the attenuation factor, A_{P}, giving,

$$A_{\mathrm{P}}(r) = \left[1 - 0.2\ln(10)\beta\int_0^r \alpha(s)Z_m^\beta(s)\,ds\right]^{1/\beta} \qquad (3.1\text{-}15)$$

3.1.1-3 Path integrated attenuation (PIA)

Here, Path Integrated Attenuation (PIA) is defined as integrated attenuation caused by precipitation particles from the radar to the surface. If $r = r_s$ at the surface, PIA is given as shown below.

$$\text{PIA} = -10\log_{10} A_\text{P}(r_s) = 2\int_0^{r_s} k(s)\,ds \qquad (3.1\text{-}16)$$

Eq. (3.1-12) can be rewritten as a function of the PIA.

$$10\log_{10} Z_m(r) = 10\log_{10} Z_e(r) - \text{PIA} + 2\int_r^{r_s} k(s)\,ds \qquad (3.1\text{-}17)$$

By substituting Eq. (3.1-15) at $r = r_s$ into Eq. (3.1-16), the following equation is obtained.

$$\text{PIA} = -\frac{10}{\beta}\log_{10}\left[1 - 0.2\ln(10)\beta\int_0^{r_s}\alpha(s)Z_m^\beta(s)\,ds\right] \qquad (3.1\text{-}18)$$

The PIA can be estimated by taking the difference between the surface backscattering cross sections with and without precipitation (surface reference technique).

3.1.1-4 Parameterization of drop size distribution function

From a mathematical point of view, $N(D)$ should be parameterized with at most two unknown parameters in order to characterize $N(D)$ deterministically from dual-frequency measurements. To keep the discussion fairly general, $N(D)$ is parameterized in the following way.

$$N(D) = N^* n(D; D^*), \qquad (3.1\text{-}19)$$

where N^* and D^* are unknown parameters and n is a function of D. By substituting Eq. (3.1-19) into Eq. (3.1-4) and (3.1-8), Z_e and k are given as below.

$$Z_e = N^* I_b(D^*), \quad I_b(D^*) = \frac{\lambda^4}{\pi^5 |K|^2}\int \sigma_b(D) n(D; D^*)\,dD \qquad (3.1\text{-}20)$$

$$k = N^* I_e(D^*), \quad I_e(D^*) = \frac{0.01}{\ln(10)}\int \sigma_e(D) n(D; D^*)\,dD \qquad (3.1\text{-}21)$$

which shows that Z_e and k can be decomposed into N^* and a function of D^* ($I_b(D^*)$ and $I_e(D^*)$).

3.1.1-5 Retrieval

3.1.1-5-1 Dual-frequency retrieval

If Z_m is available at two frequencies, N^* and D^* can be obtained by solving the following two equations.

$$10\log_{10} Z_{m1}(r) = 10\log_{10} N^*(r) + 10\log_{10} I_{b1}(D^*(r)) - 2\int_0^r k_1(N^*(s), D^*(s))\,ds \qquad (3.1\text{-}22)$$

11

$$10 \log_{10} Z_{m2}(r) = 10 \log_{10} N^*(r) + 10 \log_{10} I_{b2}(D^*(r)) - 2 \int_0^r k_2(N^*(s), D^*(s)) \, ds \quad \text{(3.1-23)}$$

The third term of the right hand side of Eq. (3.1-22) or (3.1-23) is equal to the 2-way attenuation from the storm top to range r, which implies that the retrieval should be performed sequentially from the top range bin to the gate of interest. This attenuation can be treated as a known quantity if the attenuation is expressed as a function of the DSD parameters derived at each gate. Since the solution progresses from the storm top downwards, the method is called the forward retrieval method. If an independent estimate of the PIA is available, in addition to Z_m,

$$10 \log_{10} Z_{m1}(r) = 10 \log_{10} N^*(r) + 10 \log_{10} I_{b1}(D^*(r)) - \text{PIA} + 2 \int_r^{r_s} k_1(N^*(s), D^*(s)) \, ds$$
$$\text{(3.1-24)}$$

$$10 \log_{10} Z_{m2}(r) = 10 \log_{10} N^*(r) + 10 \log_{10} I_{b2}(D^*(r)) - \text{PIA} + 2 \int_r^{r_s} k_2(N^*(s), D^*(s)) \, ds$$
$$\text{(3.1-25)}$$

Eqs. (3.1-24) and (3.1-25) instead of Eq. (3.1-22) and (3.1-23) can be used to calculate N^* and D^*. In this case, the fourth term of the right hand side of Eq. (3.1-24) or (3.1-25) is equal to the 2-way attenuation from the gate of interest (at range r) to the surface, implying that the retrieval should be done sequentially from the bottom range bin to the gate of interest. As in the forward method, if the attenuation is related to the DSD parameters at each range gate, the fourth terms can be treated as known. This method is called backward retrieval method. In reality, because of ground clutter, the fourth term cannot be calculated without some assumptions regarding the profile of the precipitation in the clutter region. Furthermore, because PIA estimates by the SRT have some error, equations (3.1-24) and (3.1-25) differ from (3.1-22) and (3.1-23), and the backward retrieval method yields different solutions from the forward retrieval method. However, the backward retrieval method is preferable, as it gives numerically stable and unique solutions, while the forward retrieval method usually has two solutions at each range bin.

In the backward retrieval method, we define $10 \log_{10} Z_{b1}$ and $10 \log_{10} Z_{b2}$ by moving the third and fourth term of the right hand side to the left hand side in Eqs. (3.1-24) and (3.1-25).

$$10 \log_{10} Z_{b1}(r) \equiv 10 \log_{10} Z_{m1}(r) + \text{PIA} - 2 \int_r^{r_s} k_1(N^*(s), D^*(s)) \, ds$$
$$= 10 \log_{10} N^*(r) + 10 \log_{10} I_{b1}(D^*(r)) \quad \text{(3.1-26)}$$

$$10 \log_{10} Z_{b2}(r) \equiv 10 \log_{10} Z_{m2}(r) + \text{PIA} - 2 \int_r^{r_s} k_2(N^*(s), D^*(s)) \, ds$$
$$= 10 \log_{10} N^*(r) + 10 \log_{10} I_{b2}(D^*(r)) \quad \text{(3.1-27)}$$

By taking the difference between Eqs. (3.1-26) and (3.1-27), we obtain:

$$10 \log_{10} Z_{b1}(r) - 10 \log_{10} Z_{b2}(r) = I_{b1}(D^*(r)) - I_{b2}(D^*(r)) \quad \text{(3.1-28)}$$

As the left hand side of Eq. (3.1-28) is known, D^* can be derived. For liquid precipitation, the right-hand side of (3.1-28) has a maximum, and Eq. (3.1-28) has generally two solutions.

3.1.1-5-2 Single-frequency retrieval

If Z_m is available only at a single frequency, we need to characterize $N(D)$ with a single parameter. This means that we assume a relationship between N^* and D^*. Once such a relation is assumed, we can translate the N^*-D^* relation to the k-Z_e relation, and the attenuation correction can be carried out by (3.1-14). If a PIA estimate by SRT ($\mathrm{PIA_{SRT}}$) is substituted into PIA in (3.1-18), the equality is generally not satisfied. This inequality is caused either by an error in the SRT or by an error in the k-Z_e relation. If the SRT is correct, the k-Z_e relation can be modified to $k = \epsilon \alpha Z_e^\beta$ where ϵ satisfies (3.1-29). This is called the α-adjustment method.

$$\mathrm{PIA_{SRT}} = -\frac{10}{\beta} \log_{10} \left[1 - 0.2 \ln(10) \beta \epsilon \int_0^r \alpha(s) Z_m^\beta(s)\, ds \right] \tag{3.1-29}$$

Once the ϵ parameter is found from (3.1-29), the Hitschfeld-Bordan solution with the modified k-Z_e relation provides the attenuation-corrected radar reflectivities. From the above attenuation correction process, k and Z_e are obtained. Then, by taking the ratio of (3.1-20) to (3.1-21), D^* can be retrieved.

$$\frac{k}{Z_e} = \frac{I_e(D^*)}{I_b(D^*)} \tag{3.1-30}$$

Generally, the right hand side of (3.1-30) is a monotonic function of D^* so that (3.1-30) has a unique solution. Since $N(D)$ is characterized by a single parameter, there is one-to-one correspondence between Z_e and D^* or k and D^*, and we can directly calculate D^* as well.

3.1.2. Overall structure of the algorithm

3.1.2-1 Algorithms

There are three kinds of Level 2 algorithms for the DPR: DPR algorithm, Ku-only (KuPR) algorithm, and Ka-only (KaPR) algorithm. The latter two are single-frequency (SF) algorithms. The DPR algorithm is a dual-frequency (DF) algorithm. The DF algorithm employs both KuPR and KaPR L2 standard products as inputs. Pixels observed by DPR can be categorized into three types: pixels in the inner swath of normal scans (observed both by KuPR and KaPR), pixels in the outer swath of normal scans (observed only by KuPR), and pixels in the interleaved scans (observed only by KaPR in the high-sensitivity mode). The KuPR algorithm is executed for pixels in both inner and outer swaths of normal scans. The KaPR algorithm is executed for pixels in the inner swath of normal scans and in the interleaved scans. The DF algorithm is executed for pixels of all the three kinds.

In the DF algorithm, pixels in the inner swath of normal scans are categorized into the dual-beam (DB) pixels. The other pixels in the DF algorithm and all the pixels in the SF algorithms are categorized into the single-beam (SB) pixels. For a SB pixel, the DF algorithm can use data in dual-frequency observations at neighboring pixels, while the SF algorithms can use data only

in the corresponding single-frequency observations. For example, by using the characteristics of the drop size distribution estimated by dual-frequency measurements at DB pixels in the inner swath, the DF algorithm can give better estimates at SB pixels in outer swath than the KuPR algorithm. Each algorithm executes data for one orbit at a time. For an orbit, only after the two SF algorithms are properly executed, the DF algorithm will be executed. The order of execution between the KuPR algorithm and the KaPR algorithm is not fixed. The algorithms are designed in such a way that the order of execution for different orbits has no restrictions within the same calendar month, but one month of data should be executed as a unit to produce proper databases.

3.1.2-2 Input/Output Files

The input and output files of the KuPR, KaPR and DF algorithms are as follows.
KuPR algorithm
> (Input) KuPR L1B standard product, Weather data file, Database file
> (Output) KuPR L2 standard product, KuPR L2 temporary file, KuPR L2 environment data

KaPR algorithm
> (Input) KaPR L1B standard product, Weather data file, Database file
> (Output) KaPR L2 standard product, KaPR L2 temporary file, KaPR L2 environment data

Dual-frequency algorithm
> (Input) KuPR L2 standard product, KaPR L2 standard product, KuPR L2 temporally file, KaPR L2 temporary file, Database file, KuPR L2 environment data, KaPR L2 environment data
> (Output) DPR L2 standard product, DPR L2 environment data, DPR L2 temporary file

The temporary files include some results of the SF algorithms, which are not written in the standard products. The temporary products can be treated as research products, once the DPR L2 standard product and other outputs are properly produced by the DF algorithm.

The environmental data include the profiles of atmospheric parameters assumed in the L2 algorithm. Because of its large volume, the ancillary environmental data are output into a separate file from the standard product.

The weather data file is prepared by converting the resolution and/or variables of weather analysis/reanalysis/forecast dataset in advance to L2 algorithm. Database files are explained later.

3.1.2-3 Modules

The framework of the L2 algorithm is shown in Fig. 3.1-1. This framework is common to the KuPR, KaPR, and DF algorithms. The main module manages the overall procedure, and it employs seven sub-modules. The main module will open and close files, call sub-modules, and read/write all the input and output files and variables. It will also terminate the algorithm. Sub-modules can read/write files and variables as long as they are permitted. As a basic rule, they should process for all the pixels in the orbit, and the order of pixels processed is not fixed (can be determined by each module). Sub-modules cannot call other sub-modules. When a sub module is terminated, the processing is returned to the main module.

Figure 3.1-1 DPR algorithm flow

3.1.2-4 Basic roles of the modules

The L2 algorithm is to numerically solve Eq. (3.1-22) or (3.1-23) for DB pixels and Eq. (3.1-30) for SB pixels to obtain N^* and D^*. The retrieval process is carried out in the Solver module, but the preparation of equations is shared by the other six modules. The PIA in Eqs. (3.1-29), (3.1-24) and (3.1-25) can be estimated in the SRT module. The DSD module is responsible for quantifying the terms in the equations such as α, β, $n(D; D^*)$, $I_b(D^*)$, and $I_e(D^*)$ based on the physical characteristics of precipitation (precipitation types and bright band information) determined by the Classification module. Z_m is converted from Z_{m0} through attenuation correction for non-precipitation particles in the Vertical Profile module and Z_{m0} is converted from received echo power in the Preparation module.

3.1.2-5 Variables

A tentative table of variables is attached to this document. The table is used for all the three algorithms in the L2 algorithms. There are two types of variables: L1B variables and L2 variables. L1B variables are just copied from the L1B standard products. L2 variables are somehow processed in the L2 algorithms. Not all but some selected variables are written in L2 standard, temporary, or environment products. A variable with scan dependence, angle bin dependence, range bin dependence, and frequency dependence is expressed as an array in the source code. Some variables may have other dimensions than scan, angle bin, range bin, and frequency. Type (bytes) of a variable can be changed when it is written into the product to save the file size. Some variables can take different values in the SF algorithms and DF algorithm. Those variables are product dependent. Product dependence and frequency dependence are explained by examples below.

- "Location of observation" is without product dependence and without frequency dependence.
- "Measured radar reflectivity factor Z_{m0}" is without product dependence and with frequency dependence.
- "Equivalent radar reflectivity factor Z_e" is with product dependence and with frequency dependence.

In the DF algorithm, variables with product dependence should be reprocessed, but variables without product dependence can be copied from SF products. Variables without product dependence and without frequency dependence should take the same value in KuPR product and KaPR product, but there is some possibility of disagreement as the KuPR algorithm and KaPR algorithm are processed independently. In the case of disagreement, a rule (e.g., KuPR algorithm is more reliable) should be prepared to determine the value in the DF algorithm.

3.1.2-6 Databases

A database is to include useful information for the algorithm, and exists as separate files from the main body of the algorithm (source code). For example, the SRT database is used in the SRT module to increase the accuracy of the PIA estimates. The L2 algorithm can refer to and update databases. The actual updating process is done not by directly modifying the database file, but by creating an intermediate file. The intermediate files are summarized and the database file is modified off line.

3.1.2-7 Look-up tables

A look-up table has a similar role with a database, but the difference is that a look-up table will basically not be updated. Therefore, we can treat the look up tables as part of the main body of the algorithm, and do not list the look-up tables as input and output files. The L2 algorithm employs a DSD look-up table and a RTM look-up table in the DSD module and the Solver module, respectively.

3.2 Main module

The basic procedure of the main module is described in 3.2.1 below. The test version before the data release in 2014 used the basic procedure. Version 3 algorithm adopts the advanced procedure 3.2.2-1. In near future, advanced procedures described in 3.2.2-2 amd 3.2.2-3 should be tested.

3.2.1 The basic procedure

In the basic procedure, sub-modules are executed in the following order, and each module is called only once. Firstly, the Preparation module is executed. This module judges the existence of precipitation, and identifies the precipitation pixels. Secondly, the Vertical profile module is executed. The ancillary atmospheric profile data are used to correct for the attenuation caused by non-precipitation particles to obtain the surface backscattering cross sections both at precipitation and no-precipitation pixels. Thirdly, the Classification module classifies each precipitation pixel into an appropriate storm type. At no-precipitation pixels, almost no processes are taken.

Fourthly, the SRT module is executed. At no-precipitation pixels, SRT database is updated based on the measurement of surface backscattering cross sections. Note that the SRT module can be executed anytime after the Vertical profile module and before the Solver module. Finally, the Solver module is executed. At no-precipitation pixels, almost no processes are taken.

3.2.2 Advanced procedure

By executing some of the modules multiple times, improvement of results is expected. Two kinds of examples are given below.

3.2.2-1 Recursive procedure

Once the basic procedure is done, the same procedure is repeated again with the parameters estimated in the first cycle. In the second cycle, for example, we can estimate the attenuation due to cloud liquid water by referring the precipitation rate estimated in the first cycle.

3.2.2-2 Parallel procedure

In the basic procedure, the sub-modules are required to determine the values of variables in charge, but sometimes they do not have enough information to estimate the values in a deterministic way. A parallel procedure allows a sub-module to give multiple estimates and to let the following sub-modules execute with multiple estimates. For example, if the precipitation type is not determined with confidence in Classification module, then the following (DSD and Solver) modules are executed with multiple assumptions of precipitation types, and the main module checks which assumption gives the vertical profiles of Z_e and the corresponding precipitation rate R in accordance with the assumed precipitation type. Thus, the precipitation type can be determined afterwards.

3.2.2-3 Additional processes

Some important processes may be missing in the basic procedure, for example, non-uniform beam filling (NUBF) correction. They should be involved in the final version of the algorithm, but currently, it has not been determined which modules are in charge of additional processes; NUBF correction can be done inside the Solver module, or should be shared with the DSD module and/or the SRT module, or a new module (Texture module) should be introduced.

3.3 Preparation module

3.3.1. Objectives and functions of the Preparation Module (PREP)

The primary purposes of the preparation module are (1) to classify the pixels into either rain or no-rain pixels, (2) to convert the received power P_r into measured reflectivity factor Z'_m without any attenuation corrections at each range bin, and (3) to calculate apparent normalized surface cross section $\sigma_m^{0}{}'$ without any attenuation correction at each pixel.

3.3.2. Algorithm descriptions of the PREP

In this section, the preparation module of Ku-band level-2 algorithm will be described in detail. As to the preparation module of Ka-band level-2 algorithm, it is almost the same with that for the Ku-band. The DPR level-2 algorithm can use level-2 products and level-2 supplementary products of both Ku-only and Ka-only algorithms. As a result, it can provide necessary information to other modules of the DPR level-2 algorithm without re-calculations.

Reading of input data

The module reads data from a Ku-band level-1B product that includes not only the radar echoes but also other variables related to the measurements such as scan time (`ScanTime`), footprint position (`Latitude`, `Longitude`), local zenith angle (`scLocalZenith`), operational mode (`operationalMode`, `acsMode`), elevation (`DEMHmean`), and data quality flag (`dataQuality`). In the case of the DPR level-2 algorithm, the module reads level-2 products and level-2 supplementary products of both Ku-band and Ka-band algorithms.

Status confirmation

The module refers to `dataQuality` of level-1B product and reflect `qualityData` of level-2 product scan by scan. If `dataQuality` is bad (not 0), level-2 values of the corresponding scan are overwritten by missing values.

Calculation of range distance (`rangeDist`)

The range distance (`rangeDist`) is defined by the distance from the satellite to each range bin along the radar beam. Each `rangeDist` is calculated from the range distance from the satellite to (the center of) the highest range bin (`startBinRange`), the number of range bins with normal sampling (`echoLowResBinNumber`), the number of range bins with over-sampling (`echoHighResBinNumber`) and the range bin size (`rangeBinSize`). Specifically, the range distance (`rangeDist`) for normal sampling ranges are calculated by using the following equation.

$$\texttt{rangeDist} = R_0 + (n-1) \times \Delta R, \quad (n = 1, 2, 3, \cdots, N)$$

The rangeDist for over sampling ranges are

$$\texttt{rangeDist} = R_0 + \{N + (m-1)\} \times \Delta R, \quad (m = 1, 2, 3, \cdots, M)$$

where

$$R_0 = \texttt{startBinRange} \text{ in L1B product}$$
$$N = \texttt{echoLowResBinNumber} \text{ in L1B product}$$
$$M = \texttt{echoHighResBinNumber} \text{ in L1B product}$$
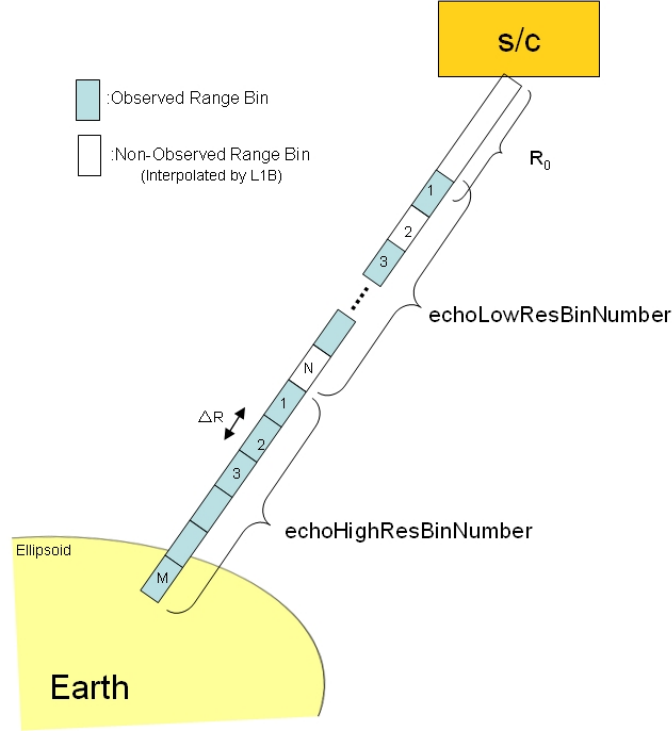$$\Delta R = \texttt{rangeBinSize} \text{ in L1B product}$$

Figure 3.3-1 Definition of `rangeDist`

Calculation of height (`Height`)

The height is defined by the vertical distance from the footprint of radar beam on the Ellipsoid to the range bin in question. In order to calculate `Height`, we define `ellipsoidBinOffset` as follows.

$$\texttt{ellipsoidBinOffset} = \texttt{scRangeEllipsoid}$$
$$- \{R_0 + (\texttt{binEllipsoid} - 1) \times \texttt{rangeBinSize}\}$$

Then, `Height` of a `binRangeNo` (as shown "p" in Fig. 3.3-3) is calculated by the following equation.

$$\texttt{Height[binRangeNo]} = \{(\texttt{binEllipsoid\_2A25} - \texttt{binRangeNo}) \times \texttt{rangeBinSize}$$
$$+ \texttt{ellipsoidBinOffset}\} \times \cos(\texttt{localZenithAngle})$$

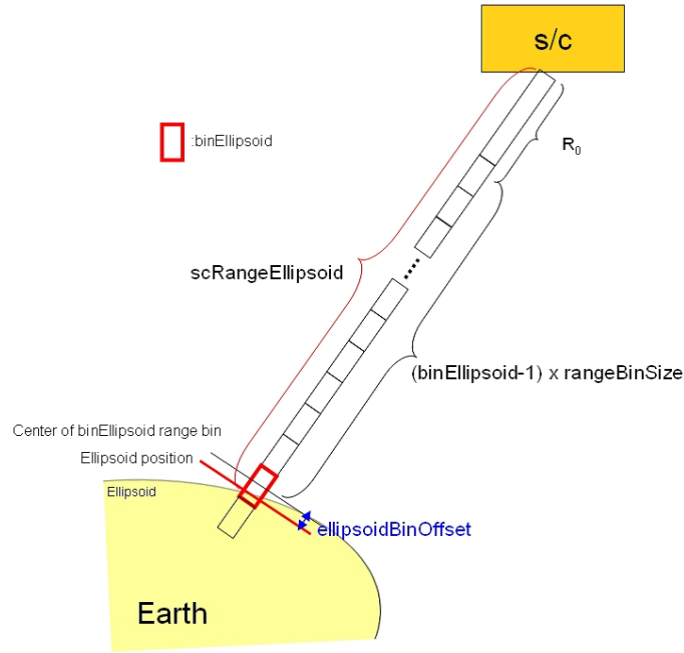where `binEllipsoid_2A25` is the Ellipsoid range bin number in level 2.

21

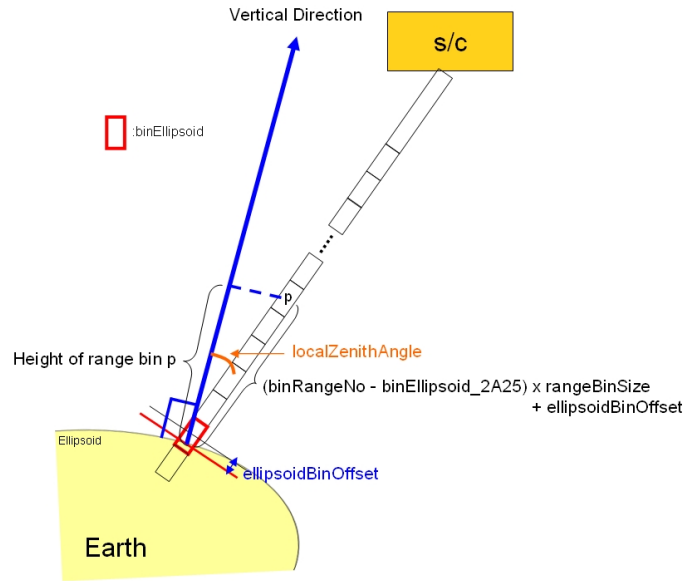Figure 3.3-2 Definition of `ellipsoidBinOffset`

Figure 3.3-3 Definition of `Height`

Extraction of level-1B range data `echoPower` and `echoFlag` of level-1B product are given at each range bin. The array size of data with range-bin dependence in Ku level-1B is 260. The array sizes of data with range-bin dependence in Ka_MS and Ka_HS level-1B are 260 and 130, respectively. On the other hand, the array size of data with range-bin dependence in Ku level-2 is 176, whereas the array sizes for range bins of Ka_MS and KA_HS level-2 are 176 and 88, respectively. The preparation module renumbers the range bins relative to the Ellipsoid

position in level-2 so that the range bin number at the Ellipsoid becomes 176 in the Ku and Ka_MS level-2 products, and 88 in the Ka_HS products. Thus, at the nadir angle bin, data from 0 km to +22 km altitude relative to the Ellipsoid are extracted.

Land surface type (`landSurfaceType`)

The land-and-ocean flag (`landOceanFlag`) of level-1B product gives land, ocean, inland water, and coast classification for each footprint. The preparation module adds surface type information for land and coast area, using footprint position (`Latitude` and `Longitude`) and an external data base. The surface type information is stored in `landSurfaceType`.

Snow- or Ice-covered area (`snowIceCover`)

In version 5, a new flag called `snowIceCover` is added to indicate the areas that are covered with surface snow or sea ice. This flag is used in the SRT module when it needs to separate different surface types and also when it collects surface scattering data to create the σ^0 database. The flag is based on NOAA/NESDIS autosnow.

Surface detection (`binRealSurface`)

The preparation module determines the surface range bin using the received power (`echoPower`), and DEM related data, such as `binDEM`, `scRangeDEM`, `DEMHmean`, `binDEMHtop`, and `binDEMHbottom` of level-1B product. The estimated surface position is stored in `binReal-Surface`.

Estimation of Clutter-free bottom (`binClutterFreeBottom`)

The range bin number of the clutter-free bottom is estimated using `echoPower` profiles. `binRealSurface` may be used as a reference of the search window. The clutter-free bottom range bin number is stored in `binClutterFreeBottom`.

Reduction of sidelobe clutter contamination

A routine to reduce the sidelobe clutter was installed in the KuPR-L2 algorithm. Fig. 3.3-4 shows a flowchart of the routine (Kubota et al. 2016). Sidelobe echoes are estimated from a statistical relationship between Normalized Radar Cross Section (NRCS) and sidelobe clutter obtained from observation data and then the routine subtracts sidelobe estimates from received power. When the sidelobe estimate is subtracted at a range bin, bit 6 in the `flagEcho` is flagged by this routine.

Calculation of Signal power (`echoSignalPower`)

Calculations of signal power are applied to all range bin data except missing data which are flagged by `dataQuality` in L1B product.

Pecho = pow(10.0,(double) `echoPower` /10)

Pnoise = pow(10.0,(double) `noisePower` /10)

23
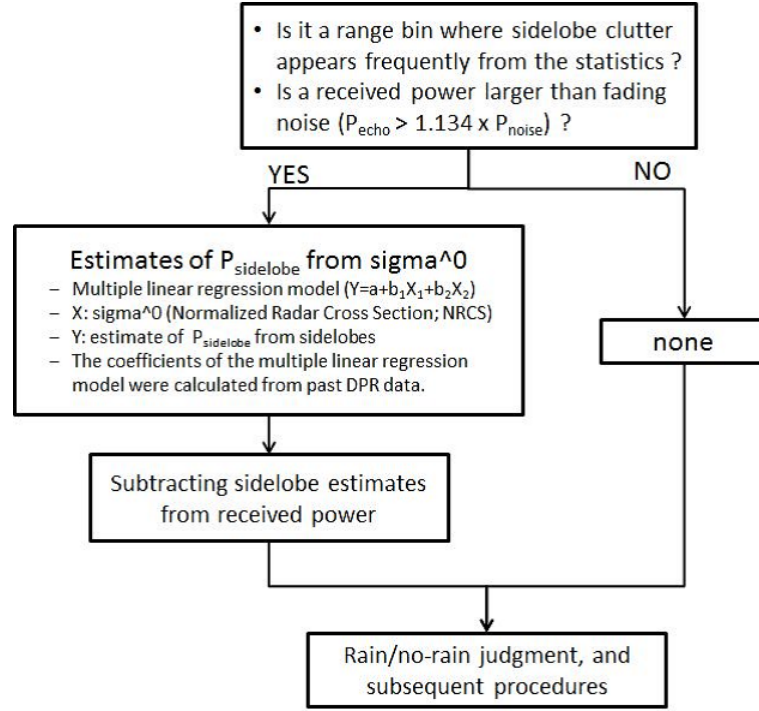
Figure 3.3-4 Flowchart of the routine to reduce sidelobe clutter installed in KuPR-L2 algorithm

Psignal = Pecho - Pnoise

echoSignalPower = 10*log10(Psignal)

where `echoPower` and `noisePower` are stored in dB unit in L1B product. If `Psignal` values are negative, missing value is stored in `echoSignalPower`.

Rain/NoRain classification (`flagEcho`, `flagPrecip`, `binStormTop`, `heightStormTop`)

Rain/NoRain classification is carried out in two steps. At first, it is done for all range bins above the `binClutterFreeBottom` except missing data which are labeled by `dataQuality` in L1B product. If `echoSignalPower` exceeds a certain threshold, it means that rain is detected for the range bin. The results of Rain/NoRain classification for range bins are stored in `flagEcho`. Then, using the surrounding `flagEcho` results, the Rain/NoRain classification for angle bin is carried out for all angle bins except missing data. The results of Rain/NoRain classification for each angle bin are stored in `flagPrecip`. The modules in the downstream in the flow chart may use the `flagPrecip` to determine the target pixels for processing. The function also detects a highest rain position in each angle bin and provides `binStormTop` and `heightStormTop`.

Calculation of Z'_m factor (`zFactorMeasured`)

Z'_m is defined as the measured reflectivity factor without any attenuation corrections. Z'_m is calculated using a radar equation at all range bins above the `binClutterFreeBottom` except

missing data which are labeled by `dataQuality` in L1B product. The result of Z'_m is stored in `zFactorMeasured`. The radar equation is as follows.

$$
\begin{aligned}
P_r &= C \cdot P \cdot L_r \cdot E \\
&= [P_t \cdot G_{\text{at}} \cdot G_{\text{ar}}] \left[\left(\frac{\lambda}{4\pi r} \right)^4 \frac{4\pi}{\lambda^2} \right] L_r \left[\frac{\pi^5}{\lambda^4} |K|^2 Z_e 10^{-18} c\tau \frac{\pi r^2 \theta_{0a} \theta_{0c}}{2^4 \ln(2)} \right] \\
&= \frac{\pi^3 c}{2^{10} 10^{18} \ln(2)} \frac{P_t G_{\text{at}} G_{\text{ar}} \theta_{0a} \theta_{0c} \tau |K|^2}{\lambda^2 r^2} L_r Z_e
\end{aligned}
$$

In the preparation module, Z'_m $(= L_r Z_e)$ is calculated by using the following equation.

$$
P_r = \frac{\pi^3 c}{2^{10} 10^{18} \ln(2)} \frac{P_t G_{\text{at}} G_{\text{ar}} \theta_{0a} \theta_{0c} \tau |K|^2}{\lambda^2 r^2} Z'_m
$$

$$
Z'_m = \frac{2^{10} 10^{18} \ln(2)}{\pi^3 c} \frac{\lambda^2 r^2 P_r}{G_{\text{at}} G_{\text{ar}} \theta_{0a} \theta_{0c} \tau |K|^2 P_t}
$$

where

r range distance (`rangeDist`)

λ wave length (`eqvWavelength` of L1B)

$|K|$ function of dielectric constant

G_t transmitter antenna gain (`txAntGain` of L1B)

G_r receiver antenna gain (`rxAntGain` of L1B)

θ_c Cross-track beam width (`crossTrackBeamWidth` of L1B)

θ_a Along-track beam width (`alongTrackBeamWidth` of L1B)

c light speed

τ transmitter pulse width (`transPulseWidth` of L1B)

P_t transmitted power (`radarTransPower` of L1B)

P_r received signal power (`echoSignalPower`)

It should be noted that $|K|$ is a constant in the preparation module. Any adjustment of $|K|$ by temperature is controlled in the solver module if necessary.

Calculation of $\sigma_m^{0\,\prime}$ (`sigmaZeroMeasured`)

$\sigma_m^{0\,\prime}$ is defined as the measured normalized surface cross section without any attenuation corrections. Calculation of $\sigma_m^{0\,\prime}$ is done for all footprints except missing data which are labeled by `dataQuality` in L1B product. The value of $\sigma_m^{0\,\prime}$ is stored in `sigmaZeroMeasured`.

$$
\sigma_m^{0\,\prime}(\theta_z) = P_{rs}(r_0) \frac{512\pi^2 \ln(2)}{P_t \lambda^2 G_t G_r} \frac{\text{loss}}{1} \frac{\cos(\theta_z) r_0^2}{\theta_a \theta_{bp}}
$$

where

$$
\theta_{bp}^{-1} = \sqrt{\theta_c^{-2} + \theta_p^{-2}}, \qquad \theta_p^{-1} = \frac{2}{c\tau} r_0 \tan(\theta_z)
$$

θ_c Cross-track beam width (`CrossTrackBeamWidth` of L1B)

θ_a Along-track beam width (`AlongTrackBeamWidth` of L1B)

P_t transmitted power (`radarTransPower` of L1B)

P_{rs} received signal power (`echoSignalPower`)

r_0 range distance from the satellite to the geographic surface (ref. `binRealSurface`)

θ_z zenith angle (`localZenithAngle`)

loss band path filter loss

λ wave length (`eqvWavelength` of L1B)

G_t transmitter antenna gain (`txAntGain` of L1B)

G_r receiver antenna gain (`rxAntGain` of L1B)

c light speed

τ transmitter pulse width (`transPulseWidth` of L1B)

3.3.3. Interfaces to other algorithms

As to the Ku-band and Ka-band level-2 algorithms, input data for this module is Ku-band and Ka-band level-1B product, respectively. For the DPR level-2 algorithm, input data for this module are level-2 products and level-2 supplementary products of both Ku-band and Ka-band. The outputs will be used by the Solver module and other modules in the DPR algorithm.

3.4 Vertical Profile Module

3.4.1 Objectives and functions of the Vertical Profile Module (VER)

The primary purposes of the VER are to read ancillary environmental data, to provide vertical profiles of the environmental parameters, to compute the path-integrated attenuation (PIA) due to non-precipitation (NP) particles, and to give radar reflectivity factors corrected for attenuation by the non-precipitation particles. The VER provides environmental information such as pressure, temperature, water vapor, and cloud liquid water at each range bin. The VER calculates the attenuation due to water vapor, molecular oxygen, and cloud liquid water.

For Ku, Ka, Ka_HS, the VER is executed using the information of the pixel lat/lon and the range bin width. For the DPR, results of the Ku, Ka, Ka_HS are introduced.

Algorithm descriptions of the VER

3.4.2 Utilization of ancillary environmental data

The VER inputs ancillary environmental data, objective analysis data by Japan Meteorological Agency (JMA) named as JMA Global Analysis (GANAL) product. By reading the ancillary environmental product, the VER provides pressure, temperature, water vapor, and cloud liquid water for each range bin. In addition, the VER computes the height of 0 degree centigrade and finds out the range bin corresponding to that height.

The horizontal resolutions of the GANAL data are 0.5 degree latitude/longitude, respectively. The pressure levels such as 1000, 925, 850, 700, 600, 500, 400, 300, 250, 200, 150, 100 hPa, and so on are converted to the height levels before the input of the algorithm. The temporal resolution is 6 hourly as 00, 06, 12, and 18Z. The VER inputs two 6-hourly files and computes the values of parameters at the time of measurement using linear temporal interpolation. We also use a linear horizontal and vertical interpolation to calculate the location of each range bin from the lat/lon's of the footprint and the satellite and the range bin height. Figuree 3.4-1 shows how this interpoloation is carried out by finding the antenna beam direction from the lat/lon information and a local zenith angle of the spacecraft and the "height" provided by the preparation module (see Section 3.3). The VER provides pressure, temperature, water vapor, and cloud liquid water at each range bin.

Calculation of attenuation by water vapor

At a frequency less than 100 GHz, the attenuation coefficient due to water vapor, $\kappa_{\mathrm{H2O}}(f)$ (dB/km) is expressed as follows (Waters 1976, Ulaby et al. 1981, Meneghini and Kozu 1990),

$$\kappa_{\mathrm{H2O}}(f) = 2f^2 \rho_\nu \left(\frac{300}{T}\right)^{3/2} \gamma_l \left[\left(\frac{300}{T}\right) e^{-644/T} \frac{1}{(494.4 - f^2)^2 + 4f^2\gamma_l^2} + 1.2 \times 10^{-6}\right]$$
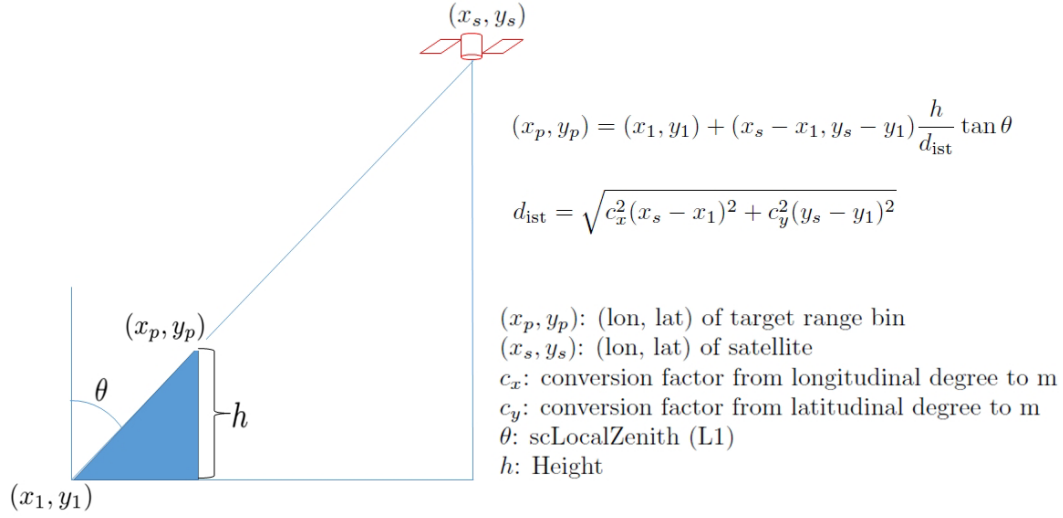
where

$$(x_p, y_p) = (x_1, y_1) + (x_s - x_1, y_s - y_1)\frac{h}{d_{\text{ist}}}\tan\theta$$

$$d_{\text{ist}} = \sqrt{c_x^2(x_s - x_1)^2 + c_y^2(y_s - y_1)^2}$$

(x_p, y_p): (lon, lat) of target range bin
(x_s, y_s): (lon, lat) of satellite
c_x: conversion factor from longitudinal degree to m
c_y: conversion factor from latitudinal degree to m
θ: scLocalZenith (L1)
h: Height

Figure 3.4-1 A concept of consideration for the antenna beam directions in the VER.

f: frequency (GHz)

ρ_ν: water vapor content (g/m3)

γ_l: parameter of line width (GHz)

T: temperature (K)

The line width parameter γ_l is given as

$$\gamma_l = 2.85\left(\frac{P}{1013}\right)\left(\frac{300}{T}\right)^{0.626}\left(1 + 0.018\frac{\rho_\nu T}{P}\right)$$

where P: pressure (hPa).

In precipitation pixels, the water vapor content provided by the GANAL may be problematic due to its relatively low resolution (0.5x0.5 deg. lat/lon). Therefore, a minimum threshold is used in the VER. The relative humidity is set to 90% when the GANAL gives a value less than 90% in precipitation pixels.

Calculation of attenuation by molecular oxygen

For attenuation by molecular oxygen, the following expression is valid for frequencies less than 45 GHz (Rosenkranz 1975, Ulaby et al. 1981, Meneghini and Kozu 1990).

$$\kappa_{\text{O2}}(f) = 1.1 \times 10^{-2} f^2\left(\frac{P}{1013}\right)\left(\frac{300}{T}\right)^2 \gamma\left[\frac{1}{(f - f_0)^2 + \gamma^2} + \frac{1}{f^2 + \gamma^2}\right]$$

where

f: frequency (GHz)

f_0: 60 GHz

γ: parameter of line width (GHz)

T: temperature (K)

Line width parameter γ is given by

$$\gamma = \gamma_0 \left(\frac{P}{1013}\right) \left(\frac{300}{T}\right)^{0.85}$$

where

$$\gamma_0 = \begin{cases} 0.59, & \text{for } 333 \leq P \text{ (hPa)}; \\ 0.59[1 + 3.1 \times 10^{-3}(333 - P)], & \text{for } 25 \leq P < 333 \text{ (hPa)}; \\ 1.18, & \text{for } P < 25 \text{ (hPa)}. \end{cases}$$

Calculation of attenuation by cloud liquid water (CLW)

For attenuation by cloud liquid water κ_{CLW} over non-precipitation pixels, cloud water contents in the ancillary environmental data product are utilized. In the cloud scheme of the JMA Climate Data Assimilation System (JCDAS) product (Onogi et al. 2007), the effective radius (r_e) of cloud liquid droplets is fixed at 15 microns. In this calculation, we assume cloud particle distribution $n_c(D)$ as mono-disperse, that is,

$$n_c(D) = N_c \delta(D - 2r_e)$$

where

D: Diameter

r_e: 15 microns

N_c: Number concentration of cloud liquid particles

For cloud liquid water content Q (kg/m3), N_c is expressed as follows,

$$N_c = \frac{3Q}{4\pi r_e^3 \rho_w}$$

κ_{CLW} is computed due to the Rayleigh scattering using $n_c(D)$. The mono-disperse assumption implies the homogeneity of the cloud distribution, although clouds generally distribute with high inhomogeneity within the grid-size of the reanalysis such as 1.25-degree latitude/longitude. Therefore, the previous formula will underestimate κ_{CLW} over precipitation pixels. In the 2A25 algorithm for the TRMM/PR, κ_{CLW} over precipitation pixels is estimated based on the result of a numerical simulation of storms with a cloud-system resolving model (CRM) that was used to create the database for the TRMM/TMI 2A12 algorithm (Iguchi et al. 2009). In their method, the attenuation due to CLW is estimated as a function of surface precipitation rate, separately for convective columns and stratiform columns. The VER adopts a method which expands Iguchi et al. (2009) and κ_{CLW} is estimated from a CLW database as a function of surface precipitation rate, precipitation type (convective or stratiform), temperature, latitude, and land surface type (Kubota et al. 2012). The CLW database was generated by 3.5 km-mesh global simulations performed using a Nonhydrostatic ICosahedral Atmospheric Model (NICAM). The NICAM is a global cloud-system resolving model (GCRM), and explicitly calculates moist convection using a cloud microphysical scheme. The NICAM data were provided by the University of Tokyo and Japan Agency for Marine-Earth Science and Technology (JAMSTEC).

3.4.3 Input Variables

Input: from MOSS or PPS

Ancillary environmental data Two 6-hourly files

      Surface: Surface pressure, Mean sea level pressure

      Pressure levels: Geopotential height, temperature, water vapor, and cloud liquid water

Input: from Preparation Module

      `Geolocation`

      `scanTime`

      `Elevation`

      `landSurfaceType`

      `localZenithAngle`

      `flagPrecip`

      `binRealSurface`

      `binStormTop`

      `heightStormTop`

      `binClutterFreeBottom`

      `sigmaZeroMeasured`

      `zFactorMeasured`

      `rangeBottom`

      `rangeTop`

      `Height`

3.4.4. Definitions of Output Variables

`airTemperature[80][49]` Temperature

`rangeZeroDeg[49]` Range bin number corresponding to the level of 0 degree centigrade.

`heightZeroDeg[49]` Height of the level of 0 degree centigrade.

`airPressure[80][49]` Pressure (hPa)

`waterVapor[80][49]` Water vapor (kg/m3)

`attenuationNPwv[80][49]` Attenuation by water vapor (dB/km)

`attenuationNPoxygen[80][49]` Attenuation by molecular oxygen (dB/km)

`cloudLiquidWater[80][49]` Cloud Liquid water content (kg/m3)

`attenuationNPclw[80][49]` Attenuation by cloud Liquid water (dB/km)

`attenuationNP[80][49]` Sum of Attenuations by water vapor, molecular oxygen, and cloud liquid water

$$\text{Atten}_{\text{NP}}(r) = \kappa_{\text{WV}}(r) + \kappa_{\text{O2}}(r) + \kappa_{\text{CLW}}(r)$$

`piaNP[80][49]` PIA by the non-precipitation particles.

$$\text{PIA}_{\text{NP}}(r) = 2 \int_0^r \text{Atten}_{\text{NP}}(s)\,ds = 2 \int_0^r \kappa_{\text{WV}}(s) + \kappa_{\text{O2}}(s) + \kappa_{\text{CLW}}(s)\,ds$$

`zFactoNPCorrected[80][49]` Radar reflectivity corrected for attenuation by the non-precipitation particles

$$Z_m(r) = Z'_m(r)/A_{\text{NP}}(r)$$

$$A_{\text{NP}}(r) = \exp(-q\text{PIA}_{\text{NP}}(r)) \quad \text{where} \quad q = 0.1\ln(10)$$

`sigmaZeroNPCorrected[49]` σ^0 corrected for attenuation by the non-precipitation particles

$$\sigma^0 = \sigma^{0'}/A_{\text{NP}}(r)$$

$$A_{\text{NP}}(r_{\text{sfc}}) = \exp(-q\text{PIA}_{\text{NP}}(r_{\text{sfc}})) \quad \text{where} \quad q = 0.1\ln(10)$$

3.4.5. Intermediate Files

Before the input of the algorithm, the pressure levels of the ancillary environmental data are converted to the height levels. In addition, the attenuations and PIA estimates by water vapor, molecular oxygen, and cloud liquid water are computed in advance.

3.4.6. Description of the Processing Procedure

Before the input of the algorithm, the pressure levels of the ancillary environmental data will be converted to the height levels. In addition, the attenuations and PIA estimates by water vapor, molecular oxygen, and cloud liquid water will be computed in advance.

For Ku, Ka, Ka_HS, the VER is executed using the information of the pixel lat/lon and the range bin width. For the DPR, calculated results of the Ku, Ka, Ka_HS are used.

3.4.7. Interfaces to other algorithms:

Input data for this algorithm is from the Preparation Module and Ancillary environmental data; the outputs will be used by the Classification module, DSD module, Solver Module and others.

3.5 Classification Module

3.5.1 Introduction

In reliable rain rate retrieval using space-borne radars, information about the drop size distribution (DSD) is necessary. DSD varies depending on the rain type. Therefore, rain type classification plays an important role in the GPM DPR algorithm. There exist two distinctive rain types, one is stratiform and the other is convective. Stratiform rain is characterized by its weakness in intensity, wide extension in area, and in many cases accompanying a bright band (BB) in radar echo. Because of the last characteristic, detection of a BB can be used for determining stratiform rain.

The rain type classification is made on pixel basis. Hence, the rain type is the same along a radar beam. Then there arises the following ambiguous situation. Suppose that, when the radar reflectivity being examined along a given radar beam, the precipitation echo happens to exist only at altitude higher than $0°$ C height. What is the rain type for this case? Is it stratiform or convective? This is a difficult question to answer. To handle such an ambiguous case, the third category of "other" type is introduced in a similar manner to the case of the TRMM PR algorithm 2A23. The third category "other" means that there exists only cloud or possibly noise when the radar echo is examined along the radar beam.

A surprise in the early TRMM PR observation was a ubiquitous shallow isolated rain system, which may be warm rain but it still remains a puzzle what it actually is. TRMM PR observation shows that shallow isolated rain is weak, which does not agree with the concept of warm rain which is thought to be very strong. There also exists shallow non-isolated rain, whose statistical properties seem to be very similar to those of shallow isolated rain. Shallow rains (both shallow isolated and shallow non-isolated rain) are marked by a shallow rain flag, `flagShallowRain`, which is independent of the rain type flag, `typePrecip`.

In the V5 classification (CSF) module, new items (`flagHeavyIcePrecip`, `flagAnvil`, `surfaceSnowfallIndex`, and `flagSurfaceSnowfall`) were added to the output fileds and a decision on winter convective type was also made. Section 3.5.5 describes these new features of V5 CSF module.

3.5.2 Objectives

The CSF module detects bright band (BB) and classifies rain into three major categories, which are stratiform, convective, and other.

3.5.3 Algorithm Principles

In single frequency CSF modules, i.e., in Ku-only and Ka-only modules, rain type classification is made by a V-method (Vertical profiling method) and by an H-method (Horizontal pattern method) (Awaka et al., 1998, 2009). The rain types by the V-method and H-method are unified,

and the Classification (CSF) module outputs the unified rain type, which consists of three major categories; stratiform, convective, and other.

In the dual frequency algorithm of GPM DPR, however, rain type classification is made by a new method called measured dual frequency ratio (DFR_m) method (Le and Chandrasekar, 2013a, 2013b) and by using the single frequency result from the Ku-only module. The DFR_m method is a kind of vertical profiling method, and classifies rain type into stratiform, convective and transition. Though transition is a new type, it is not a major category. The rain types by the DFR_m method and those by the Ku-only module are unified. Three major categories, after the unification of rain types of DFR_m method and Ku-only results, are again stratiform, convective and other.

3.5.3-1 Single frequency: V-method

In the single frequency V-method, detection of BB is made first. Detection of BB is made by examining the vertical profile of the radar reflectivity factor (Z) and see if the vertical profile of Z satisfies certain conditions which are typical to the profile of Z when BB exists. When BB is detected, rain type is stratiform if the reflectivity factor in the rain region does not exceed a special convective threshold. When BB is not detected, and the reflectivity factor exceeds a conventional convective threshold, rain type is convective. When rain type is neither stratiform nor convective, the rain type is "other" in the V-method.

3.5.3-2 Single frequency: H-method

In the H-method, a horizontal pattern of a representative radar reflectivity factor is examined. Here the representative reflectivity factor means the maximum value of reflectivity factor in the rain region along the considering radar beam. Rain type is classified using a modified University-of-Washington convective/stratiform separation method (Steiner et al. 1995, Yuter and Houze 1997). In the H-method, rain type is again classified into three categories: stratiform, convective and other. In the H-method, detection of convective rain is made first. If the rain type is not convective, the rain type is stratiform unless the reflectivity factor is very small, being almost identical to noise. If rain type is neither convective nor stratiform, the rain type is other.

3.5.3-3 Dual frequency: DFR_m method

In the dual frequency module, in place of the V-method, DFR_m method is used for rain type classification and for BB detection in the inner swath. The DFR_m method uses the difference between measured Ku-band Z in dB and the measured Ka-band Z in dB. To make the BB detection reliable, BB detected by the DFR_m method and that by the Ku-only algorithm are unified in the dual frequency CSF module. Rain types by the DFR_m method are stratiform, convective and transition. In the outer swath in which only Ku-band data is available, rain type and BB are the copy of those in the Ku-only module. The DFR_m method is also used for

handling HS data by interpolation, which is made vertically and horizontally. In the vertical interpolation, the Ka-band data with a 125 m interval is interpolated from a 250 m interval HS data. In the horizontal interpolation, four Ku-band data adjacent to the HS pixel are used for the interpolation of the corresponding Ku-band data at the HS pixel.

3.5.4 Actual Algorithm (Data Processing)

3.5.4-1 Single frequency processing

In Ku-only and Ka-only algorithms, BB detection is based on a search of typical BB peak by examining the range profile of radar reflectivity along a given antenna beam. This method is effective to the Ku-band data which show clear BB peaks. In the case of Ka-band, however, since a clear BB peak is not expected, detection of BB is not effective.

3.5.4-1-1 Selection of pixels to be processed:

- Skip the process for the pixel if no precipitation echo exists in Ku-band and Ka-band data. This judgment can be made by examining a flag from the PRE module, `flagPrecip`.
- Skip the process for the pixel if the quality flag of Ku-band and/or that of Ka-band shows that the pixel is a bad pixel or that the data is missing. This judgment can be made by examining a flag from the PRE module, `qualityData`. (It is assumed here that the information about missing data is also available from the `qualityData` flag.)

3.5.4-1-2 Determination of range where precipitation echoes exist:

- Determination of the echo top and the echo bottom, where the echo top is given by `rangeStormTop` from the PRE module and the echo bottom is given by `binClutterFree-Bottom` from the PRE module.

3.5.4-1-3 Detection of bright band (BB) by the single frequency method

- Set the BB search window using `rangeZeroDeg` from the VER module. The BB search window ranges from $\mathtt{rangeZeroDeg} - 4$ to $\mathtt{rangeZeroDeg} + 8$ with a 250 m interval, where the center of the BB window is $\mathtt{rangeZeroDeg} + 2$ which is about 0.5 km below the 0 degree height. This window range is reasonable from TRMM PR experience and many other radar observations (unfortunately, Ka-band radar data may not exhibit a clear BB peak, but the BB search window can be the same for the Ku-band and Ka-band). Experience shows that BB peak appears about 0.5 km below the 0 degree height.

  Detection of BB is made using the NP-attenuation corrected radar reflectivity factors, `zFactorNPCorrected`, from the VER module, where NP-attenuation means attenuation due to non-precipitation particles.

  Detection of BB can be made by two methods: one is a vertical method and the other is a (horizontal) texture method. The vertical method examines the profile of radar reflectivity

35

factor. If the profile of the radar reflectivity satisfies certain conditions which characterize BB, it is determined that there exists BB. The above characteristic conditions are different between Ku-band and Ka-band. In the Ku-band, a sharp BB peak should be observed in the profile of radar reflectivity. In the Ka-band, however, a clear BB peak may not be observed, but there must be a detectable characteristic change in the slope in the radar reflectivity profile near the BB.

The (horizontal) texture method detects BB by examining nearby pixels. The (horizontal) texture method is effective for detecting a BB smeared by slanted beam observation.

When BB is detected, the upper boundary of BB (i.e., `rangeBBTop`) and the lower boundaries of BB (i.e., `rangeBBBottom`) are determined. The lower boundary of BB is detected first. The lower boundary of BB is defined as the point where there is the largest change in the slope of Z in the region just below the BB peak. This definition is very close to that by Fabry and Zawadzki (1995). The upper boundary of BB is determined by finding the following two points A and B:

Point A: where there is the largest change in the slope of Z in the upper region of BB peak.

Point B: where Z becomes smaller than Z at the lower boundary of BB for the first time when Z is examined upward in the upper part of BB starting from the BB peak.

When points A and B are the same, the upper boundary of BB is defined as the point A (which is the same as the point B in this case). When points A and B are different, the upper boundary of BB is defined as either A or B that is closer to the BB peak. The definition of the upper boundary is the one which is somewhere in between the definition by Fabry and Zawadzki (1995) and that by Klaassen (1998).

The width of BB (`widthBB`) is computed by the following empirical formula:

$$\texttt{widthBB} = [(\texttt{rangeBBBottom} - \texttt{rangeBBTop}) \times 125 - L\sin(\theta_z)]\cos(\theta_z) \qquad [\text{m}]$$

where θ_z is the local zenith angle, and L is given below:

$$L = L_0 F / \cos^2(\theta_z)$$

Here L_0 (=5000 [m] tentatively) is the footprint size of antenna beam, and F is an empirical factor ($F = 0.5$, tentatively). When the above equation gives `widthBB` $< 250\cos(\theta_z)$ [m], the width is set to `widthBB` $= 250\cos(\theta_z)$ [m]. When BB is detected, the following quantities are computed or given and written to the output of the single frequency CSF module.

  - `flagBB`: This flag indicates that BB is detected. (`flagBB` > 0 when BB is detected.)
  - `rangeBBPeak`: Range bin number of BB peak. In the case of Ku-band, it is simple and straight forward. In the case of Ka-band, BB peak may not be clear, and the peak position

may be displaced from that of Ku-band. Nevertheless, a simple peak search method is used also at Ka-band.

- `rangeBBTop`: Range bin number of BB top.
- `rangeBBbottom`: Range bin number of BB bottom.
- `heightBB`: Height [m] of BB which corresponds to `rangeBBPeak`.
- `widthBB`: Width of BB [m].
- `qualityBB`: Quality flag of BB detection. Details are still TBD. The flag `qualityBB` is meaningful when BB is detected. Tentatively in V4, `qualityBB`=1 always when BB is detected (which means that the quality of all the detected BB is good).

3.5.4-1-4 Rain type classification by the single frequency method

In each single frequency CSF module, that is, in Ku-only or Ka-only CSF module, rain type classification is made by two methods: one is a V-method and the other is an H-method. V- and H-methods classify rain into three categories; stratiform, convective and other. The rain types by these two methods are unified, and each single frequency CSF module outputs the unified rain type, which consists of three major categories; stratiform, convective and other.

3.5.4-1-4-1 V-method

In the V-method, stratiform rain is detected first.

- When BB is detected, the rain type is stratiform.
- When BB is not detected, the rain type is convective if one of the following conditions is satisfied. Otherwise, the rain type is other.

(a) The radar reflectivity factor, `zFactorNPCorrected`, in the valid range between `rangeStormTop` and `binClutterFreeBottom` exceeds a threshold, which is 39 dBZ in both Ku-band and Ka-band.

(b) Storm top in Ka- or Ku-band is very high (> 15 km (TBD)). (Not implemented in V4.)

3.5.4-1-4-2 H-method

In the H-method, horizontal texture of the maximum value of `zFactorNPCorrected` in the rain region along each radar beam, Z_{max}, is examined. A modified University of Washington convective/stratiform separation method is applied to the horizontal extent of Z_{max}. When one of the following conditions is satisfied, the considering pixel is a convective center:

(a) Z_{max} in the pixel exceeds a convective threshold, or

(b) Z_{max} in the pixel stands out against that in the surrounding area.

Rain type of the convective center is convective, and the rain type of pixels adjacent to the convective center is convective. If the rain type is not convective, and if Z_{max} is not small

enough to be considered as noise, the rain type is stratiform. If $Z_{\max}$ is very small, being almost identical to noise, the rain type is other.

3.5.4-1-4-3 Shallow rain and small cell-size rain

Detection of shallow rain is also made independently of the above mentioned methods of rain type classification. When the following condition is satisfied, it is judged as shallow rain, which will be marked by an internal flag:

$$\mathtt{heightStormTop} < \mathtt{heightZeroDeg} - \mathrm{margin}$$

where margin is currently 1000 m.

Shallow rain is separated out into shallow isolated and shallow non-isolated by examining the horizontal extent of shallow rain. In the rain type unification, both shallow isolated and shallow non-isolated are classified as convective. (It should be noted that in the TRMM PR rain type classification algorithm 2A23 V7, all the shallow isolated is convective, but shallow non-isolated can be either stratiform or convective.)

Detection of rain having small cell size is also made independently. The rain having small cell size is classified as convective in the unification of rain type.

3.5.4-1-4-4 Unification of rain type by the single frequency method

Rain types by the V-method and by the H-method are unified, and the CSF module outputs the unified rain type, which consists of three major categories of stratiform, convective and other. The unified rain type is written to the flag `typePrecip`. There are many rain type sub-categories depending on the combination of V- and H-mehod results. The unified rain type is expressed by eight digit numbers as follows:

> `typePrecip` = 1xxxxxxx   for stratiform rain,
>   2xxxxxxx   for convective rain,
>   3xxxxxxx   for other rain,

where xxxxxxx varies depending on subcategories. Details will be given elsewhere. In a computer program, the three main categories of unified rain type can be obtained easily from `typePrecip`. Let Type be the integer variable for the main category, for example, then the main category can be obtained by one of the following codes:

> Type = `typePrecip` / 10000000 (in Fortran),
> Type = `typePrecip` / 10000000; (in C)

3.5.4-2 Dual frequency processing

In the dual frequency processing, a newly developed DFR_m method is used for the detection of melting layer (ML) and rain type classification. Details of DFR_m method is given in 3.5.4-2-3. The concept of ML has a meaning wider than that of BB. In other words, BB which appears

in the stratiform rain is a subset of ML. Since BB is a subset of ML, the DFR_m method can be used for the detection of BB. In the dual frequency processing, the DFR_m result and the Ku-only result are merged.

3.5.4-2-1 Detection of bright band (BB) by the dual frequency method

In the dual frequency method, BB detected by the Ku-only method and ML by the DFR_m method are compared. Firstly, ML detected by the DFR_m method is regarded as BB. Together with BB detected by the Ku-only method, the median of the height of BB is computed in one scan of data. When the considering height deviates from the median to a large extent, it is judged that the considering BB is not a true BB and the BB decision is rejected.

If BB is detected by both the Ku-only and the DFR_m methods at a given angle bin, it is judged that the height of BB is the height which is closer to the median of BB height.

When BB is thus detected, properties of BB such as height, width, etc., for matched beam data are then determined by using the profile of Z at Ku-band only, because Z at Ku-band shows a clear BB peak but in most cases Z at Ka-band doesn't. Because only the Ku-band Z profile is used for the determination of BB properties, NS outputs of the BB properties in the inner swath are copied to the corresponding MS outputs.

Since the concept of ML is wider than that of BB, and the upper and lower bounds of ML are different from those of BB in general, the following two items are added to the output of dual frequency CSF module (for both MS and HS data):

- `rangeDFRmMLTop`: Range bin number of ML top. (The name was `rangeDFRmBBTop` in V3.)
- `rangeDFRmMLBottom`: Range bin number of ML bottom. (The name was `rangeDFRmBBBottom` in V3.)

Names of the other BB related items are the same to those of single frequency items.

In the HS mode data processing, detection of BB is made by the DFR_m method only.

3.5.4-2-2 Rain type classification by the dual frequency method

As is shown in the next 3.5.4-2-3, the DFR_m method classifies rain into the following three types: stratiform, convective, and transition, the latter of which is a new rain type. The rain type by the DFR_m method is merged with the rain type by the Ku-band H-method, and the dual frequency CSF module outputs unified rain type which consists of the following three major types: stratiform, convective and other.

The unified rain type is expressed by eight digit numbers as follows:

typePrecip = 1xxxxxxx for stratiform rain,

2xxxxxxx for convective rain,

3xxxxxxx for other rain,

where xxxxxxx varies depending on subcategories. In a computer program, the three main categories of unified rain type can be obtained easily from typePrecip. Let Rtype be the

integer variable for the main category, for example, then the main category can be obtained by one of the following codes:

Rtype = `typePrecip` / 10000000 (in Fortran),

Rtype = `typePrecip` / 10000000; (in C)

The rain type by the DFR_m method is expressed in the 2nd digit of typePrecip. Hence the rain type by the DFR_m method, if we denote it by DFRmRtype for example, can be obtained as follows:

DFRmRtype = MOD(`typePrecip`, 10000000) / 1000000 (in Fortran),

DFRmRtype = (`typePrecip` % 10000000) / 1000000; (in C).

When rain exists, DFRmRtype takes one of the following values:

1: stratiform,

2: convective,

4: transition,

5: when stratiform is changed to convective by the extended DFRm method explained in 3.5.5-2,

8: DFR_m method skipped at Part B in Fig. 3.5-3 (shown later).

9: DFR_m method skipped at Part A in Fig. 3-5-3 (shown later).

3.5.4-2-3 Detail description of DFR_m method

Dual-frequency precipitation radar DPR offers Ku and Ka band dual-frequency observations along the vertical profile which allow us additional information to investigate the microphysical properties using the difference between two frequency observations or so-called measured dual-frequency ratio (DFR_m) defined as

$$\text{DFR}_m = 10 \log_{10}(Z_m(K_u)) - 10 \log_{10}(Z_m(K_a)) \tag{3.5-1}$$

where Z_m is measured reflectivity. DFR_m profile holds rich information to assist in precipitation type classification and melting layer detection. There are two main functions of DFR_m method in classification module: (1) precipitation type classification, and (2) melting layer detection. Correspondingly, there are two models developed for dual-frequency profile classification method. Figure 3.5-1 shows typical vertical profiles of reflectivity and DFR_m for stratiform and convective rain. These profiles are observations from airborne precipitation radar.

3.5.4-3 Precipitation type classification model

Precipitation type classification model classifies stratiform, transition, and convective rain types. The main parameter used in the model is DFR_m and its vertical variation. In order to quantify the features of DFR_m, a set of DFR_m indices are defined. Let $V1$ be

$$V1 = \frac{\text{DFR}_{ml}(\max) - \text{DFR}_{ml}(\min)}{\text{DFR}_{ml}(\max) + \text{DFR}_{ml}(\min)} \tag{3.5-2}$$
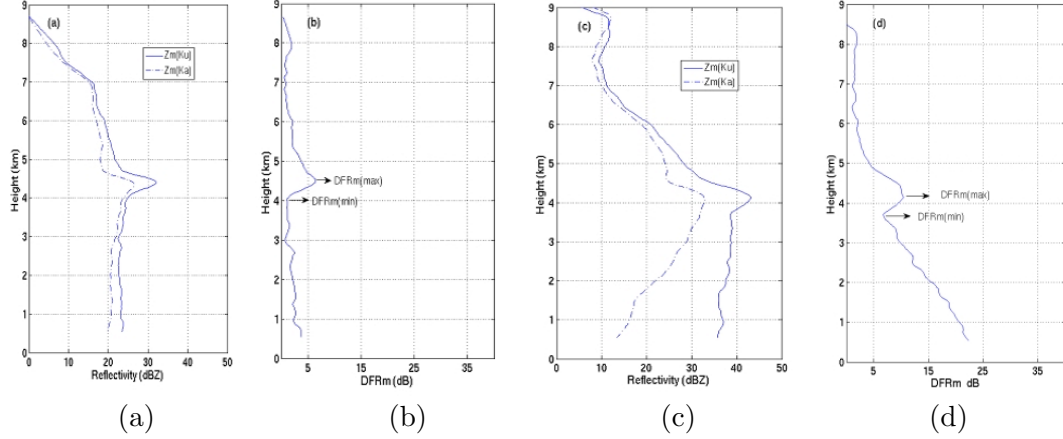
Figure 3.5-1. Typical vertical profiles for stratiform (a)(b) and convective (c)(d) rain. (a)(c) Measured reflectivity at Ku and Ka band; (b)(d) DFR_m. DFR_m(max) and DFR_m(min) marked on (b) and (d) are local max and min value.

DFR_m(max) and DFR_m(min) are shown in figure 4.2.3-1. $\mathtt{DFR}_{ml}$ used in (3.5-2) means DFR_m in linear scale. Let V2 be the absolute value of the mean slope for DFR_m below the local minimum point

$$V2 = \mathrm{abs}(\mathrm{mean}(\mathtt{DFR}_m\mathrm{slope})) \tag{3.5-3}$$

Both $V1$ and $V2$ are normalized values and not dependent on the height or depth of the melting layer. $V1$ values are normally larger for stratiform rain than for convective rain and $V2$ values are larger for convective than for stratiform rain. To further enlarge the difference between stratiform and convective rain types, a third index $V3$ is defined as

$$V3 = \frac{V1}{V2} \tag{3.5-4}$$

The index $V3$ is an effective parameter and provides a separable threshold for performing precipitation type classifications. Extensive statistic studies are performed on index $V3$ using both airborne radar data and GPM real data. Cumulative density function (CDF) of index $V3$ is calculated for stratiform and convective database separated using Ku only classification algorithm. Separable thresholds of C1 and C2 can be found on index $V3$ for stratiform and convective rain types with 70% of CDF. In other words, for stratiform rain: $V3 > C2$; convective rain: $V3 < C1$; transition type: $C1 \leq V3 \leq C2$. $C1$ is smaller than $C2$. "Transition" type is neither a stratiform, nor a convective rain type, but a type transitioning from stratiform to convective rain. Figure 3.5-2 shows histogram of index $V3$ and its cumulative density function calculated using total of 73 storms data with 121859 vertical profiles. Table 3.5-1 shows the thresholds of $C1$ and $C2$ used in the current version. In the future, further adjustment of $C1$ and $C2$ is needed. Figure 3.5-3 illustrates the block diagram for precipitation type classification model that used in the current version.
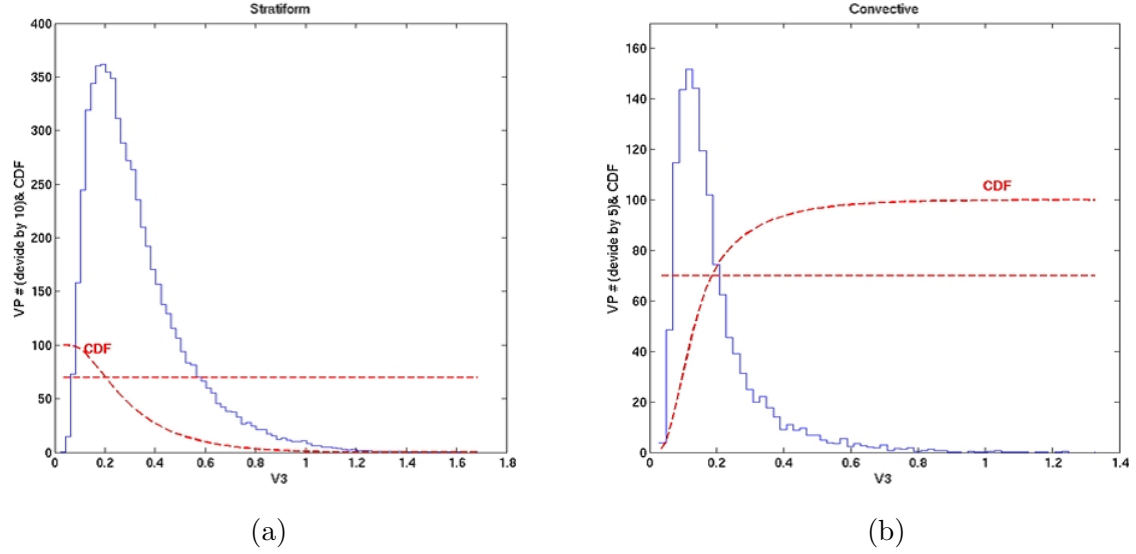
41

Figure 3.5-2. Histogram of DFR$_m$ index $V3$ with CDF line for (a) stratiform rain and (b) convective rain calculated using total of 121859 vertical profiles from GPM real data.

Table 3.5-1. C1 and C2 thresholds used in precipitation type classification model

70% CDF	121859 vertical profiles of GPM data
C1	0.18
C2	0.20

3.5.4-4 Melting layer detection model

Melting layer detection model detects melting layer top and bottom height for each vertical profile. The main parameter used in the model is DFR$_m$ profile and its vertical variation. When DFR$_m$ pair as shown in Fig. 3.5-1 is detected, the melting layer top is defined as the height at which the slope of the DFR$_m$ profile hits a peak value. The melting layer bottom is defined as the height at which the DFR$_m$ profile has a local minimum value. The dashed lines in Fig. 3.5-4 show an illustration of melting layer top and bottom detected.

The criteria described above have been compared with other existing criteria in the literature using different radar parameters. Tilford et al. (2001) used the gradient of reflectivity (Z_m) to detect the bright band top and bottom for stratiform rain type. The linear depolarization ratio (LDR) has been pointed out by many researchers as an important signature in melting phase detection, with certain thresholds determined for different hydrometeor particles (Smyth et al., 1998; Bandera et al., 1998; Tan and Goddard, 1995; Hines, 1983). Typical vertical profiles of reflectivity as well as the corresponding velocity for stratiform and convective type were extensively studied by Fabry and Zawadzki, (1994). Baldini and Gorgucci (2006) mentioned
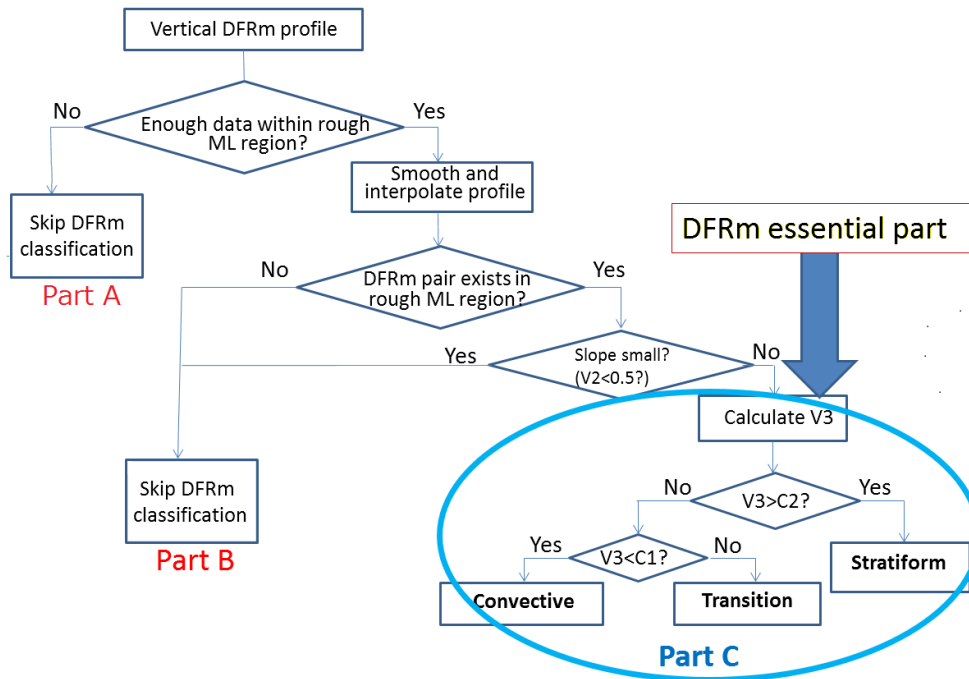
Figure 3.5-3. Block diagram of precipitation type classification model.
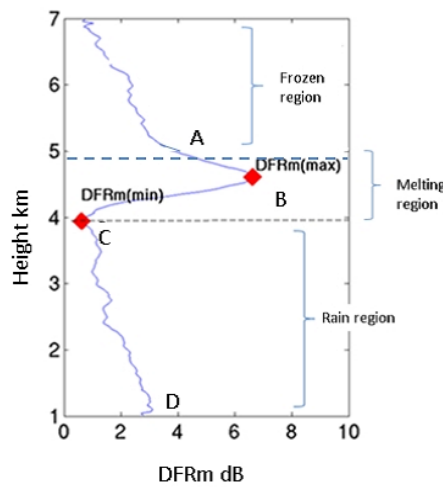

Figure 3.5-4. Schematic plot of DFR_m profile with key points A, B, C, and D. Point A: slope of DFR_m has peak value. Point B: local maximum of DFR_m. Point C: local minimum of DFR_m. Point D: DFR_m value near surface.

that the rapid change of the hydrometeor fall velocity is an implication of the melting layer. The curvature of velocity was used by Zrnic et al. (1994) in characterizing the melting boundaries. Klaassen (1988) found that the melting bottom can be detected by maximum of velocity. Figure 3.5-5 shows a schematic plot of the comparisons between melting layer detection criteria in DFR_m method and other existing criteria. The comparison results using airborne radar data

are listed in Table 3.5-2. From the table, estimations from the DFR_m method match best with velocity based criteria with normalized bias of 1.3% and 2.2% for melting layer top and bottom respectively. The DFR_m method also compares well with the LDR criteria, with a -28 dB threshold, the bias between these two criteria is around -2.8%. Details can be found in Le and Chandrasekar (2012). Figure 3.5-6 shows a profile comparison between DFR_m method and LDR as well as velocity criteria using APR-2 observations. Figure 3.5-7 is the block diagram of melting layer detection model used in the current version of DFR_m classification method.
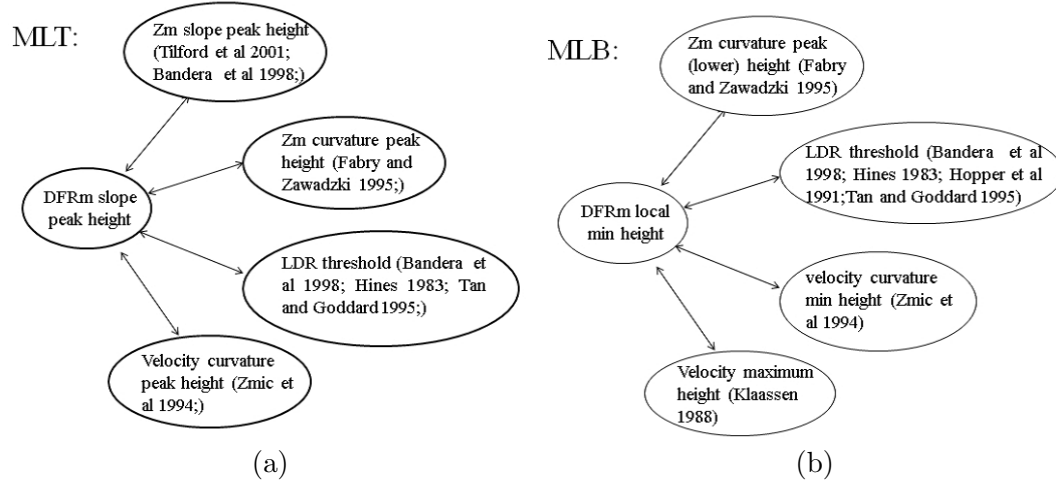

Figure 3.5-5. Schematic plots of some current criteria for melting layer boundaries detection and their possible relations with melting layer detection model used in the DFR_m method. (a) melting layer top criteria; (b) melting layer bottom criteria.

Table 3.5-2. Comparisons of melting layer boundaries between different criteria for NAMMA, GRIP and Wakasa Bay data.

	Criteria	DFR_m slope peak (NAMMA)		DFR_m slope peak (GRIP)		DFR_m slope peak (Wakasa Bay)	
		NB	NSE	NB	NSE	NB	NSE
Melting layer top comparison	Z_m slope peak	-2.6%	3.6%	-2.5%	3.6%	-4.9%	6.6%
	Z_m curvature peak	1.6%	3.3%	1.5%	3.0%	2.8%	5.2%
	LDR	-2.8%	4.5%	-3.3%	4.2%	-6.0%	7.2%
	Velocity curvature peak	-1.3%	3.6%	-1.4%	3.7%	-1.9%	5.6%

	Criteria	DFR_m slope peak (NAMMA)		DFR_m slope peak (GRIP)		DFR_m slope peak (Wakasa Bay)	
		NB	NSE	NB	NSE	NB	NSE
Melting layer bottom comparison	Z_m curvature peak	4.3%	5.5%	3.7%	5.0%	4.3%	6.9%
	LDR	4.5%	5.9%	4.0%	5.4%	5.4%	11.2%
	Velocity curvature min	2.2%	4.9%	1.7%	4.4%	-0.08%	7.0%
	Velocity max	1.6%	5.9%	1.9%	4.3%	-2.6%	13.9%
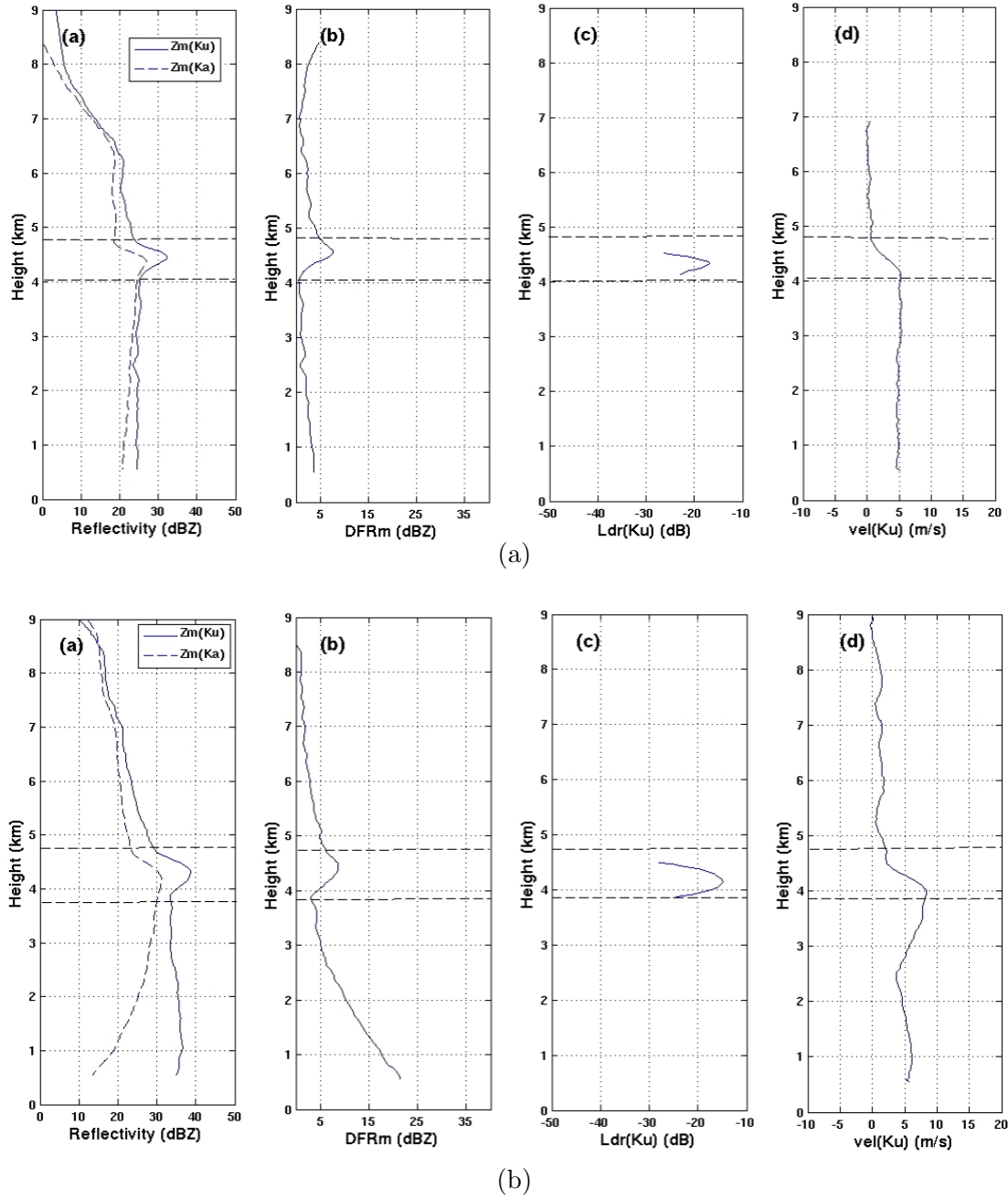
Figure 3.5-6. Sample profile from airborne radar data. Top row (stratiform rain): (a) $Z_m(\text{Ku})$ and $Z_m(\text{Ka})$; (b) DFR_m; (c) LDR; (d) Velocity;Dashed lines are melting layer top and bottom decided by the DFR_m method. Bottom row (convective rain): (a) to (d) are the same as in top row.

3.5.5 New features in the V5 CSF module

Most of new features in the V5 CSF module described in this section arise from the advantage of dual frequency data processing.
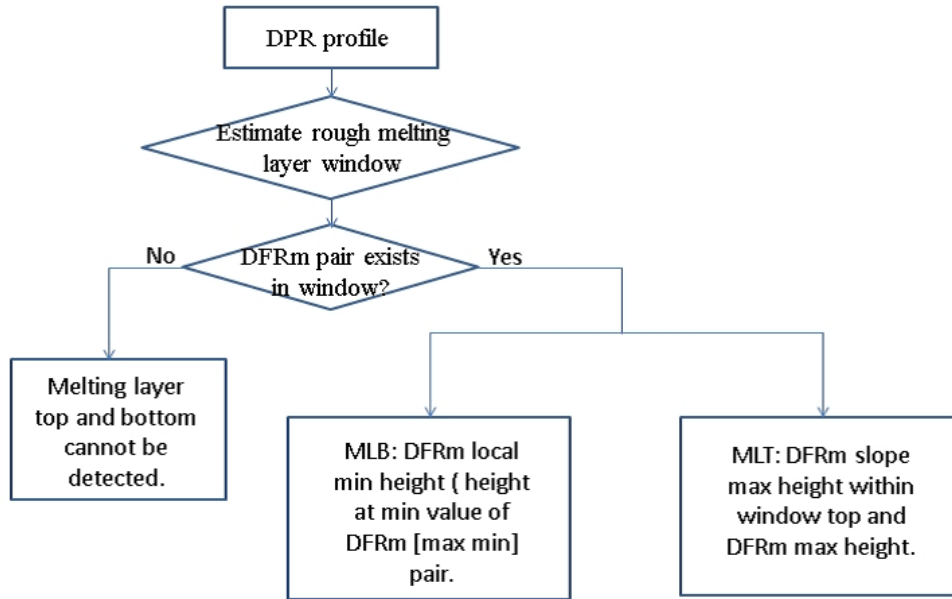
Figure 3.5-7. Block diagram of melting layer detection model for DFR_m method.

3.5.5-1 `flagHeavyIcePrecip`

This flag indicates that a Heavy Ice Precipitation (HIP) is detected in the upper region of storm where the temperature is lower than -10 degrees in Centigrade. Here, HIP is defined as precipitation consisting of ice particles which produces a large measured Z factor (Z_m) and/or produces a large DFRm. Detection of HIP, proposed by Dr. Iguchi, is made by examining Ku Z_m and Ka Z_m in the single frequency modules and by additionally examining DFRm in the dual frequency module. The following values of `flagHeavyIcePrecip` are devised to distinguish by which decision HIP is detected (see Figure 3.5-8.)

Default value: `FlagHeavyIcePrecip` $= 0$ (HIP not detected, including the case of missing)

Ku-band decision (Ku NS)

   If KuPR's $Z_m > 45$ dBZ, then `flagHeavyIcePrecip` $= 12 = $ 0x0C

   Else if KuPR's $Z_m > 40$ dBZ, then `flagHeavyIcePrecip` $= 8 = $ 0x08

   Else if KuPR's $Z_m > 35$ dBZ, then `flagHeavyIcePrecip` $= 4 = $ 0x04

Ka-band decision (Ka MS)

   If KaPR's $Z_m > 40$ dBZ, then `flagHeavyIcePrecip` $= 3 = $ 0x03

   Else if KaPR's $Z_m > 35$ dBZ, then `flagHeavyIcePrecip` $= 2 = $ 0x02

   Else if KaPR's $Z_m > 30$ dBZ, then `flagHeavyIcePrecip` $= 1 = $ 0x01

DPR decision

   Outer swath: The same as the outer swath value of Ku NS.

   Inner swath: The addition of the above value of Ku NS, that of Ka MS, and the following value of DFRm decision:
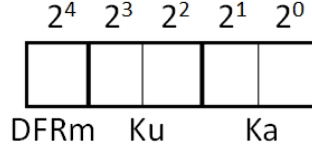
46

2^4 2^3 2^2 2^1 2^0

DFRm   Ku   Ka

Figure 3.5-8. Bit assignment of `flagHeavyIcePrecip`

KuPR's $Z_m > 27$ dBZ and DFRm > 7 dB, then `flagHeavyIcePrecip`$= 16 =$0x10

3.5.5-2 Detection of winter convection

Detection of winter convection is made by examining DFRm at the storm top and its vicinity. The basic idea is that a large DFRm near the storm top in winter may indicate the convective nature of precipitation. Since DFRm is examined, the method in this section can be called an 'extended DFRm method'. It is found that the above `flagHeavyIcePrecip` plays an important role in the detection of convective precipitation in winter. When the following conditions are satisfied, it is judged that the winter convection is detected by the extended DFRm method (See DFRmRtype in 3.5.4-2-2.).

(1) The estimated 0C height is lower than or equal to 1 km. (Winter condition.)

(2) `flagHeavyIcePrecip` > 0 is found near the considering pixel. Here, the term 'near' means the inner swath region within -3 to $+3$ scans measured from the considering pixel's scan number (see Figure 3.5-9).

(3) Examine the DFRm of 5 consecutive range bins starting from storm top towards downward direction. At three or more range bins, the following condition is satisfied:

$$\text{DFRm at } x > \frac{2.5 - 0.8}{5.0} + 0.8$$

where x is the relative range bin number counted downward from the storm top.

(4) If Z_m at any of the examining range bins exceeds 35 dBZ, the process of detecting winter convection is skipped because such a large Zm near the storm top may mean the existence of BB.

3.5.5-3 `flagAnvil`

Since the Ku-band PR turns out to have a higher sensitivity, the Ku-band PR data can be used for the detection of 'Anvil'. For the definition of 'Anvil', we need to introduce cloud top and cloud bottom, where cloud top is identical with storm top and cloud bottom means the range bin below which no rain bins continue to some extent. (When precipitation exists, the cloud top always exists but the cloud bottom does not always exist.) As shown in Figure 3.5-10, when the cloud bottom is 500 meters higher than the estimated 0C height, it is defined that the 'Anvil' exists. If there does not exist any precipitation echoes below the 'Anvil', it is judged that the
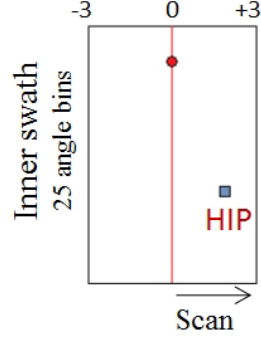
Figure 3.5-9. Nearness of the considering pixel (marked by a circle) to the pixel of `flagHeavyIcePrecip` > 0 (marked by a square)

'Anvil' type 1 is detected. If precipitation echoes exist below the 'Anvil', but if the no rain interval between the cloud bottom and the top of precipitation echoes below the 'Anvil' exceeds 1 km, it is judged that the 'Anvil' type 2 is detected (see Figure 3.5-10(b)). The V5 CSF module detects type 1 'Anvil' and type 2 'Anvil' only. The possible values of `flagAnvil` are as follows:

`flagAnvil`=1: type 1 'Anvil' is detected (there is no rain echo below the 'Anvil'),

=2: type 2 'Anvil' is detected (there exists rain echoes below the 'Anvil',

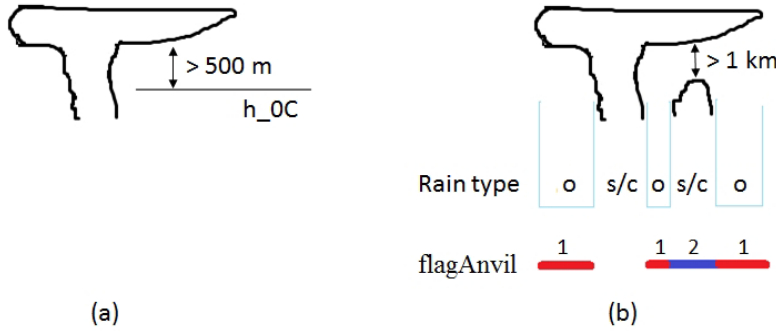=0: 'Anvil' is not detected (including the case of data missing).

Figure 3.5-10 Definition of 'Anvil'

3.5.5-4 Surface snowfall

The V5 CSF module introduces a process which determines whether the precipitation at the surface is snow or rain. The process has been developed by Dr. Chandra's group. The process outputs the following two variables. (Though the decision is made in the CSF module, the two variables are available in the Experimental output fields of dual frequency MS.)

`surfaceSnowfallIndex`: If this index exceeds a predetermined threshold, it is judged that the surface precipitation is snow.

`flagSurfaceSnowfall`: This flag takes the following two values.

$$\texttt{flagSurfaceSnowfall} = \begin{cases} 1: & \text{The surface snowfall is possible,} \\ 0: & \text{The surface snowfall not detected.} \end{cases}$$

48

3.5.6 Snow and rain feature on measured dual-frequency ratio (DFRm) profile

Figure 3.5-11 (a) shows the first snow observation caught by GPM DPR with overpass #000272. On that overpass, there are snow, stratiform and convective rain precipitation within 160 scans (around 800 km) range. In the figure, A, B and C indicates the location of snow, stratiform and convective rain. In order to study vertical profile feature for these different precipitation types, we study averaged reflectivity as well as measured dual-frequency ratio profile for snow, stratiform and convective rain. The vertical profile is calculated from linear averaging of reflectivity at corresponding heights. If data in a pixel is missing or below noise level, it is not considered in the average. Figure 3.5-11 (b) shows the averaged reflectivity profile for snow at Ku-, Ka- band and a measured dual-frequency ratio. As expected, reflectivity at Ku- band is, most of the time, below 25 dBZ. However, the difference between Ku- and Ka- band (indicated by DFRm) is several dBs, even when reflectivity at Ku- band remains a relatively small value. DFRm values increase obviously when it comes toward the surface mainly due to the aggregation of the snow particles. Figure 3.5-11 (c) shows an averaged vertical profile for stratiform rain. The bright band is obvious from Ku- band reflectivity. Values of DFRm below the melting region (or the bright band) are very small indicating that attenuation at Ka- band is very small when reflectivity at Ku- band is less than around 25 dBZ in the rain region. DFRm values are quite constant with respect to height. In contrast, DFRm values above melting layer is several dBs and DFRm slope is noticeable, which is similar to the snow profile in figure 2 (b). For convective rain, from figure 1 (d), the maximum of reflectivity at Ku- band is equal or larger than 35 dBZ, while DFRm values are considerable in the rain region. Large DFRm values in rain are contributed from both attenuation difference and the non-Rayleigh scattering effect, while the former factor plays a more important role. DFRm slope for convective rain is large mainly due to large attenuation different change when it comes toward the surface.

One of the features for a convection storm is that it is normally formed at a higher altitude in the atmosphere (except for some warm rain or orographic rain) compared to stratiform and snow precipitation.

Based on analysis above, three ingredients of DFRm, maximum value of reflectivity at Ku-band, as well as storm top height become important, then are used in the development of the algorithm to identify surface snowfall. To avoid calibration issues, we use the slope of DFRm instead of DFRm itself.
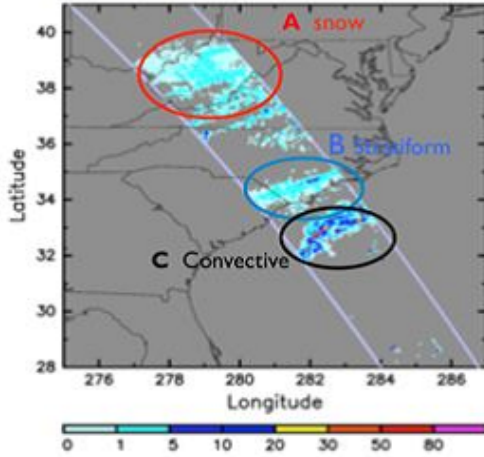
3.5.7 Algorithm description

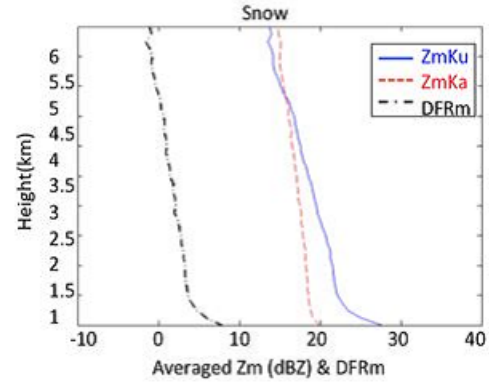Snow index (SI) is carefully chosen from the features discussed in section 1. The definition of SI is

$$\mathrm{SI} = \frac{\mathrm{mean}(|\mathrm{DFRm_{slope}}|)}{\mathrm{Zmku_{max}} \times \mathtt{Storm\_top\_height}} \quad (1)$$
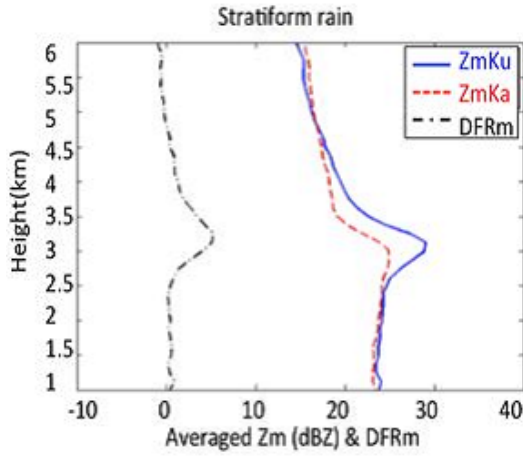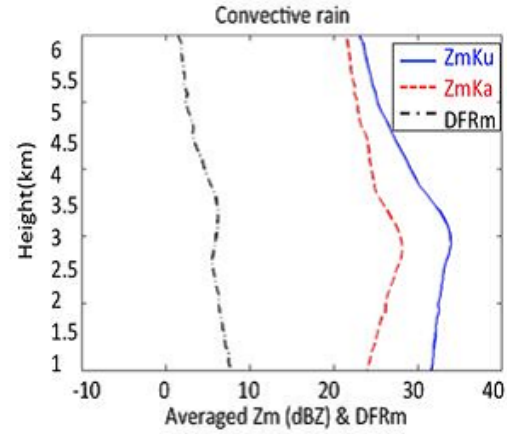
Figure 3.5-11. GPM DPR overpass of rainfall rate on March 17, 2014 (#000272). Circled A, B and C represents snow, stratiform rain, and convective rain. (b) Averaged reflectivity profiles as well as dual-frequency ratio profile for snow. (c) Same as (b) for stratiform rain. (d) Same as (b) for convective rain.

DFRm slope (in dB/km) is used instead of DFRm value due to its immunity to calibration change. Zmku_{max} (in dBZ) represents maximum of reflectivity at Ku-band along the profile. Storm_top_height represents altitude of storm top in km. In general, absolute value of DFRm slope in the numerator of (1) is larger for snow than for stratiform rain. Zmku_{max} value in the denominator is larger for convective rain than for snow, while storm top height in the denominator is lower for snow and stratiform rain than for convective rain. Therefore, SI is expected to be a larger value for snow profile than for rain. In the algorithm, we use the normalized value of Zmku_{max} and Storm_top_height. A statistics study of snow index is performed on large scale of

50

GPM DPR vertical profiles. A total of 353166 rain profiles and 4935 snow profiles are used in this study. Rain profiles are chosen from tropical regions during the summer season and snow profiles are chosen from northern Europe and the northern US in the winter season. Information of 0 degree isotherm is used in profile selection. Figure 3.5.12 shows the histogram of snow index (SI) defined in (1) for snow and rain profiles respectively. In general, as expected, snow index is larger for snow profiles. The cumulative density function (CDF) is calculated for rain, and illustrated as a blue dashed curve in figure 8, while red dashed curve represents 1- CDF for snow profiles. At around 97% of CDF (or 1-CDF), SI index can separate snow and rain profiles. In other word, 97% of snow profiles have SI > 17, while 97% of rain profiles have SI <= 17. The statistics study considers calibration changes that will be applied to version 5 of the GPM DPR level 2 algorithm.
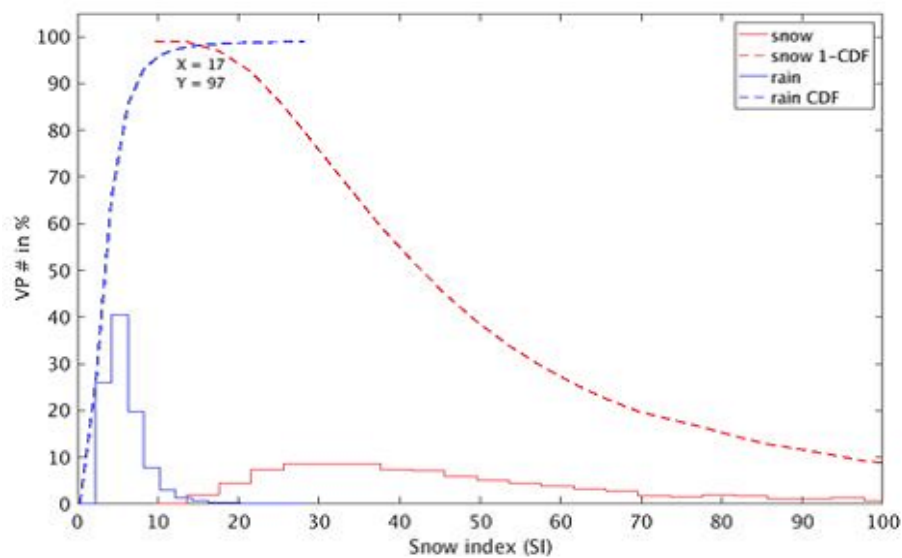
Figure 3.5-12. Large scale study of snow index using GPM DPR profiles. Histogram of snow index for rain (blue) and snow (red). Blue dashed curve is the cumulative density function (CDF) for rain. Red dashed curve is 1- CDF for snow.

Figure 3.5-13 shows the flow chart of the surface snowfall identification algorithm that uses snow index. Besides snow index, other auxiliary information such as 0 degree isotherm and clutter free height are used in the algorithm. Although 0 degree isotherm (or surface temperature) plays an important role in snowfall detection, its accuracy is a challenge for space-borne weather radars such as GPM. Therefore, in this algorithm, 0 degree isotherm is not the dominant parameter but rather a constraint parameter. Snow index is calculated for profiles with 0 degree isotherm heights not higher than 10 range bins (1.25 km) above clutter free height. This serves more like a sanity check to filter out nonsense profiles.

Figure 3.5-13. Flowchart to perform surface snowfall identification in profile classification module of GPM DPR level 2 algorithm.
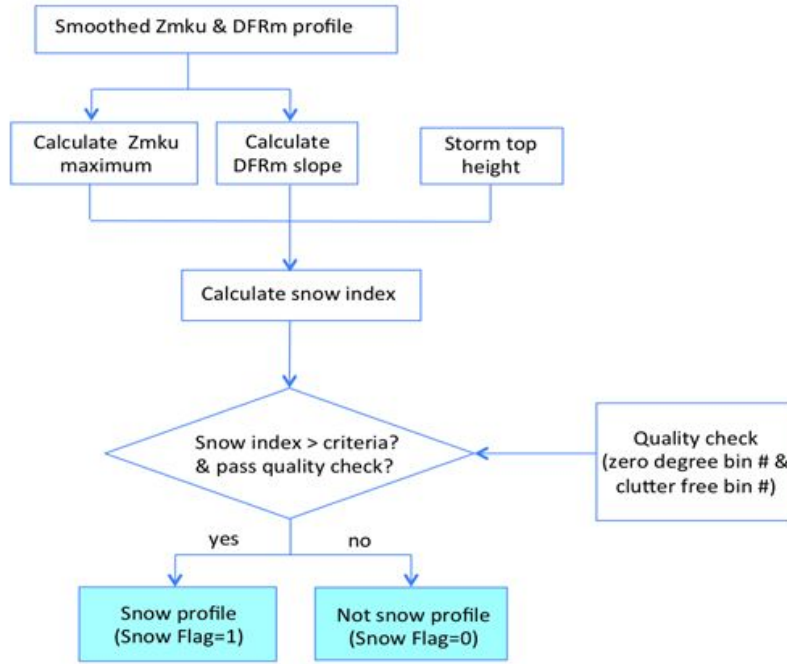
3.5.8 Enhancement of GPM DPR level 2 dual-frequency classification module

In the current DPR level 2 classification module, the vertical profile is classified as either stratiform, convective or other type following the TRMM legacy. However, GPM orbits cover both cold and tropical regions. It is reasonable to add snow flag to vertical profiles that indicate whether there is snow on the surface or not. The surface snowfall identification algorithm takes advantage of dual-frequency measurements from GPM DPR, thus it provides a new approach to detect snow other than the method using surface temperature or surface echo. The algorithm outputs `flagSurfaceSnowfall` and `surfaceSnowfallIndex` to each vertical profile in the DPR inner swath. This snow flag provides useful information for microphysics retrieval for other modules such as the solver module. Therefore, this algorithm enhances the current dual-frequency classification module in GPM DPR level 2 algorithm and has been implemented as an experiment version.

3.5.9 Detection of orographic rain (optional)

In the CSF module, detection of orographic rain will be tried in the future. Unfortunately, however, detection of orographic rain would require research works.

3.5.10 Input and Output Variables

Input Variables

From Preparation (PRE) module:

lat

lon

ScanTime information (`Year`, `Month`, `DayOfMonth`, `Hour`, `Minute`, `Second`, Millisecond, `DayOfYear`, `SecondOfDay`)

elevation

landSurfaceType

localZenithAngle

flagPrecip

binRealSurface

binStormTop

heightStormTop

binClutterFreeBottom

sigmaZeroMeasured

rangeBottom

rangeTop

Height

echoSignalPower

zFactorMeasured

From Vertical (VER) module:

airTemperature

binZeroDeg

zFactorNPCorrected

heightZeroDeg

flagEcho (R/W) (This flag marks possible sidelobe clutter positions.)

qualityData (R/W)

From Solver (SLV) module:

zFactorNPCorrected (For convective decision by the V-method in the
single frequency Ku- or Ka-loop)

Output Variables

flagBB [4 byte integer (can be 2byte integer)]

binBBPeak [2 byte integer]

binBBTop [2 byte integer]

binBBBottom [2 byte integer]

heightBB [4 byte real]

widthBB [4 byte real]

qualityBB [4 byte integer (can be 2 byte integer)] (Currently tentative values are
set, that is, when BB is detected, qualityBB=1 (meaning good) always.)

53

typePrecip [4 byte integer]

qualityTypePrecip [4 byte integer (can be 2 byte integer)] (Currently tentative values are set, that is, when rain exists, qualityTypePrecip=1 (meaning good) always.)

flagShallowRain [4 byte integer (can be 2 byte integer)]

binDFRmMLTop [4 byte integer] (dual frequency MS and HS output fields only)

binDFRmMLBottom [4 byte integer] (dual frequency MS and HS output fields only)

flagHeavyIcePrecip [1 byte integer]

flagAnvil [1 byte integer]EEingle frequency Ku NS and dual frequency NS output fields onlyEE

flagSurfaceSnowfall [1 byte integer] (Experimental output field of dual frequency MSEE

surfaceSnowfallIndex [4 byte real] (Experimental output field of dual frequency MSEE

3.5.11 Relation to other modules

The Classification (CSF) module uses data from the Preparation (PRE) module and the vertical (VER) module. Each single frequency CSF module uses data from the corresponding Solver (SLV) module in the 2-nd part of (a kind of iteration) loop for convective decision by the V-method. The output data from the CSF module is used by the Solver (SLV) module.

3.6 DSD module

3.6.1 Objective

The objective of DSD module is to set the physical variables of precipitation particles (especially, density, dielectric constants, and falling velocity), to parameterize $N(D)$ (in other words, to set $n(D; D^*)$), and to set the R-D_m relationship.

3.6.2 Processes

The following processes are common to single- and dual-frequency algorithms.

3.6.2-1 Target pixels and range bins

Pixels with precipitation are processed. Range bins from the storm top range bin to the land surface range bin (including those without precipitation and those with ground clutter) are processed. In dual-frequency algorithm, range bins from the higher storm top range bin of the two frequencies to the lower land surface range bin of the two frequencies are processed.

3.6.2-2 Nodes and the physical temperature and phase of the particles

Five range bins are selected as nodal bins and designated as nodes A through E. Simultaneously, the physical temperature of particles (particle temperature) and the phase of particles are set. Particle temperature is related to the dielectric constants and it is not necessarily the same with air temperature. The dielectric constant is dependent on the precipitation types and the detection of bright band.

3.6.2-2-1 Stratiform precipitation with bright band

The range bin that corresponds to the upper edge of bright band is node B, the range bin at the peak of bright band is node C, and the range bin at the lower edge of bright band is node D. Between node B and node D, particle temperature is set to 0°C. Above node B, the particle temperature is basically the same with ambient air temperature, but is 0°C if the air temperature is higher than 0°C. Below node D, the particle temperature is basically set to the same with the air temperature, but 0°C if the air temperature is lower than 0°C. The range bin with particle temperature closest to −20°C corresponds to node A, and that closest to 20°C is node E. At and above node A, the phase of precipitation is *Solid*. At and below node D, the phase of precipitation is *Liquid*. At other range bins, below node A and above node D, the phase of precipitation is *Mixed* (Solid and Liquid).

3.6.2-2-2 Stratiform precipitation without bright band

The process is the same as 3.6.2-2-1, but the nodes B, C, and D are at the range bin corresponding to 0°C.

3.6.2-2-3 Convective precipitation or other-type precipitation

The process is the same as 3.6.2-2-2.

3.6.2-3 Assumption of precipitation particles

A precipitation particle is modeled as a spherical particle composed of liquid water, solid water, and air. Its diameter (or drop size) is designated as D_b [mm], and its density as ρ_b [g/cm^3]. The volume ratios of liquid water, solid water, and air to the particle are P_w, P_i, and P_a, respectively. The following equation always holds.

$$P_w + P_i + P_a = 1 \tag{3.6-1}$$

The densities of liquid water, solid water, and air are ρ_w, ρ_i, ρ_a, respectively. Then, the density of the particle can be given as below.

$$\rho_b = P_w\rho_w + P_i\rho_i + P_a\rho_a \tag{3.6-2}$$

Generally, we can assume $\rho_w = 1.0$ (g/cm^3). ρ_i is also constant (for example, $\rho_i = 0.92$). Moreover, ρ_a can be regarded to be 0 (g/cm^3) for simplicity. With these constant values, Eq. (3.6-2) can be simplified to (3.6-3).

$$\rho_b = P_w + 0.92P_i \tag{3.6-3}$$

3.6.2-4 Setting of volume ratio and density

3.6.2-4-1 Liquid phase particle

Obviously, $P_w = 1$, $P_i = P_a = 0$, $\rho_b = 1.0$ (g/cm^3).

3.6.2-4-2 Mixed phase particle

First, P_w is set based on Awaka's model or TRMM/PR's experience. Then, ρ_b can be calculated by the following empirical equation.

$$\rho_b = \sqrt{P_w} \tag{3.6-4}$$

Then, P_i can be calculated by Eq. (3.6-2) with $\rho_a = 0$.

$$P_i = \frac{\rho_b - P_w\rho_w}{\rho_i} \tag{3.6-5}$$

3.6.2-4-3 Solid phase particle

First, ρ_b is set, for example, $\rho_b = 0.10$ (g/cm^3). As $P_w = 0$, P_i can be calculated by Eq. (3.6-5).

3.6.2-5 Dielectric constants

ε_b is calculated by mixing rule, for example, given in Eq. (3.6-6).

$$\frac{\varepsilon_b - 1}{\varepsilon_b + U} = P_w \frac{\varepsilon_w - 1}{\varepsilon_w + U} + P_i \frac{\varepsilon_i - 1}{\varepsilon_i + U} + P_a \frac{\varepsilon_a - 1}{\varepsilon_a + U} \qquad (3.6\text{-}6)$$

where U is given as below,

$$U = \begin{cases} 2.0 & \text{if } \rho_b \leq 0.09 \text{ g/cm}^3, \\ 2.0 e^{13.0(\rho_b - 0.09)} & \text{if } \rho_b > 0.09 \text{ g/cm}^3. \end{cases} \qquad (3.6\text{-}7)$$

ε_w and ε_i are dielectric constants of water and ice and are functions of particle temperature, and ε_a is dielectric constants of air. As ε_a is approximated to 1, Eq. (3.6-6) can be simplified to Eq. (3.6-8).

$$\frac{\varepsilon_b - 1}{\varepsilon_b + U} = P_w \frac{\varepsilon_w - 1}{\varepsilon_w + U} + P_i \frac{\varepsilon_i - 1}{\varepsilon_i + U} \qquad (3.6\text{-}8)$$

3.6.2-6 Falling velocity

Falling velocity V_b of the particle can be given as below.

$$V_b = 3.3 \times [\rho_b - \rho_a]^{1/2} \qquad \text{if } \rho_b \leq 0.05 \text{ g/cm}^3; \qquad (3.6\text{-}9a)$$

$$V_b = 8.8 \times [0.1 D_b(\rho_b - \rho_a)]^{1/2} \qquad \text{if } 0.05 \text{ g/cm}^3 < \rho_b \leq 0.3 \text{ g/cm}^3; \qquad (3.6\text{-}9b)$$

$$V_b = \frac{\rho_b^{1/3} - 0.3^{1/3}}{1.0 - 0.3^{1/3}}(V_R - V_{b0.3}) + V_{b0.3} \quad \text{if } 0.3 \text{ g/cm}^3 < \rho_b \leq 1.0 \text{ g/cm}^3. \qquad (3.6\text{-}9c)$$

where D_m is a diameter after melting, and the relationship between D_b and D_m are as follows.

$$D_b = D_m \rho_b^{-1/3} \qquad (3.6\text{-}11)$$

In Eq. (3.6-9c), $V_{b0.3}$ is the falling velocity calculated in Eq. (3.6-9b) with $\rho_b = 0.3 \text{ g/cm}^3$.

3.6.2-7 Drop size distribution function

3.6.2-7-1 Liquid phase

Gamma distribution function may be most commonly used for the drop size distribution function in liquid phase. The function is given as below.

$$N(D) = N_0 D^\mu \exp\left[-\frac{(3.67 + \mu)D}{D_0}\right], \qquad (3.6\text{-}12)$$

where μ should be known. N^* in (3.1-19) corresponds to N_0, D^* to D_0, and n is given as Eq. (3.6-13).

$$n(D; D_0) = D^\mu \exp\left[-\frac{(3.67 + \mu)D}{D_0}\right], \qquad (3.6\text{-}13)$$

3.6.2-7-2 Mixed phase and solid phase

It is assumed that when all the particles are melted to liquid particles, the drop size distribution obeys Eq. (3.6-12). With Eq. (3.6-11), Eq. (3.6-12) can be expressed by D_b and ρ_b.

$$N(D_b)\,dD_b = N_0 \rho_b^{(\mu+1)/3} D_b^{\mu} \exp\left[-\frac{(3.67+\mu)D_b\rho_b}{D_0}\right] dD_b \qquad (3.6\text{-}14)$$

Eq. (3.6-14) can be modified to Eq. (3.6-15), if we consider the difference of number density caused by the difference of falling velocity as Non-break up and Non-coalescence model (N/N model) assumes.

$$N(D_b)\,dD_b = N_0 \rho_b^{(\mu+1)/3} D_b^{\mu} \frac{V_R(D_m)}{V_b(D_b)} \exp\left[-\frac{(3.67+\mu)D_b\rho_b}{D_0}\right] dD_b \qquad (3.6\text{-}15)$$

3.6.2-8 R-D_m relation

R-D_m relations are assumed for stratiform and convective rain separately to calculate k and Z_e for a given R at both Ka and Ku bands. In version 3 algorithm, default k-Z_e relations were given as the basic relations to constrain the DSD parameters. However, since these relations were derived from the R-Λ relation (Kozu et al. 2009) by assuming a power law between k and Z_e, the resultant k-Z_e relations did not reproduce the original R-Λ relations exactly. The discrepancy was apparent espcially in heavy rainfall cases for KaPR and solid particles, and caused a serious error in the algorithm. Since the R-D_m relation is directly derived from the R-Λ relation without approximation, we have consistent DSD parametes to relate k, Z_e at both freqencies and R.

The actual R-D_m realtions adopted are $R = 0.401\epsilon^{4.649}D_m^{6.131}$ for stratiform precipitation and $R = 1.370\epsilon^{4.258}D_m^{5.420}$ for convective precipitation, where ϵ is an adjustment factor and is the same with ϵ used in version 03 and in the TRMM/PR algorithm. The same equations are used for all range bins irrespective of its "phase", while D_m is defined for particle size when melted.

3.6.3 Phase

An index called "phase" is introduced. "phase" is an integer-type variable. If "phase" is equal to or greater than 200, particles are in liquid phase, and the difference between the value of "phase" and 200, i.e., (phase$-$200), indicates the particle temperature in unit of degrees C. For example, if "phase" is 210, the particle temperature is 10 degrees C. If "phase" is between 100 and 200, particles are in a bright band. 100 is for the top of bright band, 150 is for the peak of bright band, and 200 is for the bottom of bright band, where all particles are melted in liquid phase. 125 and 175 are used for intermediate positions, but other numbers between 100 and 200 are not used. If "phase" is smaller than 100, particle is partly or fully frozen, and the difference between "phase" and 100 means particle temperature in unit of degrees C. For example, if "phase" is 80, particle temperature is -20 degrees C.

3.6.4 DSD database

ϵ used in the R-D_m relations was assumed to follow the log-normal distribution. In the version 04, the average (μ) and the standard deviation (σ) of $\log_{10} \epsilon$ is set at 0 and 0.1, respectively. In the version 05, the statistics of ϵ is calculated based on the outputs of ϵ at dual-frequency pixels by the dual-frequency algorithm. The average and the standard deviation of $\log_{10} \epsilon$ are calculated for each precipitation type (stratiform, convective), for each land surface type (land, ocean, all), each 5 by 5 degree grid box, and each month. Not only grid values but global values are prepared. The purpose of the DSD database is to make estimates by KuPR algorithm be closer to those by the dual-frequency algorithm. DSD database is applied only to single-frequency pixels (all pixels of the single-frequency algorithms and pixels in outer swath or in interleaved scan of the dual-frequency algorithm). In the dual-frequency pixels of the dual-frequency algorithm, μ and σ is set 0 and 0.1 same as in the version 04.

3.7 Surface Reference Technique for DPR

3.7.1. Objective of the algorithm

The primary purpose of the surface reference technique (SRT) is to compute the path-integrated attenuation (PIA), or simply path attenuation, using the radar return from the surface. The SRT rests on the assumption that the difference between the measurements of the normalized radar surface cross section, σ^0 or NRCS, in dB, within and outside the rain provides an estimate of the PIA.

For the dual-frequency Precipitation Radar (DPR), the method is to be applied to the Ku-band as well as the Ka-band and Ka-band high sensitivity (KaHS) data. The basic set of output products for each of the channels (Ku, Ka and KaHS) consist of the path attenuation estimate (when rain is present) and an associated reliability. As in the TRMM algorithm 2a21, version 7, the primary output for each channel will be an effective or 'best' PIA estimate. In addition, however, path attenuation estimates corresponding to specific types of surface reference data are also generated. These are described below. The standard PIA estimates will be produced by processing the data from the 3 channels (Ku, Ka, Ka_HS) independently. However, to take advantage of the correlation in the NRCS at the two frequencies, dual-frequency-derived path attenuations at Ku- and Ka-band will also be generated in the inner swath. These are referred to as the DPR-Ku and DPR-Ka estimates.

For each 'channel' (Ku, Ka, KaHS, DPR-Ku, DPR-Ka), a spatially or temporally-averaged estimate of the rain-free normalized radar surface cross section (σ^0 or NRCS) is used as a reference value for computing the PIA. For the DPR channel, the rain-free reference data is obtained from a difference between the Ka- and Ku-band σ^0 data. The algorithm computes up to six estimates of path attenuation, corresponding to six different σ^0 reference estimates for each of the five channels. An effective PIA is obtained by weighting the individual estimates by a factor that is inversely proportional to the variance of the estimate. The reference estimates are described below:

Along-track Spatial Average: The along-track spatial average is obtained from an average of the N_s most recent rain-free σ^0 measurements at same angle bin and with the same surface type (nominally, $N_s = 8$) as the rain pixel of interest.

Hybrid or Cross-Track: The hybrid reference data set is generated from a quadratic fit of the along-track spatial average data over the angle bins within the cross-track swath. This is explained below in more detail. For the Ku-band, separate fits are done for the inner ($|\theta| \leq \theta_0$) and outer swath ($|\theta| > \theta_0$) where $\theta_0 \approx 9°$.

Temporal Average: The temporally averaged data, which are given in the form of look-up tables, presently consists of statistics (sample mean, sample mean square and number of data points) of rain-free σ^0 data at $0.5° \times 0.5°$ latitude-longitude cells, separated into incidence angle.

60

The look-up tables have been derived from the Ku, Ka, KaHS and differential (σ^0(Ku)- σ^0(Ka)) data categorized into 25, 13, 12, and 13 angle bins, respectively.

In version 5 of the algorithm, each of these files is further subdivided into 5 surface-dependent look-up tables that correspond to ocean, land, coast, sea-ice and snow-covered land surface types for a total of 20 look-up tables for each 3-month period (DJF, MAM, JJA, SON). It is worth noting that a sixth category, which includes all surface types, is also generated, for a total of 24 look-up tables. The eall-surface typesf table is used only when the number of data points for the surface type of interest is smaller than the minimum number, nominally set to 20. Note that version 4 uses only 3 surface types (ocean, land and coast); in version 5, sea-ice and snow-covered land surface types have been added.

Forward-Backward Processing

Different estimates for along-track and cross-track (or hybrid) methods are obtained from forward and backward processing. This provides up to six estimates - *Forward Along-track, Forward Cross-track, Backward Along-track, Backward Cross-track, and two types of Temporal reference files* - for each rain observation. Note that the hybrid/cross-track estimates are only available over ocean since the fitting procedure does not work well over land. (Cross-track fitting over land might be effective for the difference field, σ^0_{NR}(Ku) $- \sigma^0_{NR}$(Ka). Whether such an estimate is to be used is to be determined.) The different reference estimates are filtered according to various criteria. For example, an along-track estimate isn't used if the location of the reference data is too far from the observed rain point. A temporal estimate is considered invalid if the number of rain-free observations at a particular angle for the reference cell is too few. The surviving estimates are weighted by the inverse of their associated variance. The weighted estimates are combined to yield an effective PIA for each of the channels, (pathAtten_Ku, pathAtten_Ka, pathAtten_KaHS). The individual estimates, (PIAalt_Ku, PIAalt_Ka, PIAalt_KaHS), and their weights, (PIAweight_Ku, PIAweight_Ka, PIAweight_KaHS) are included in the output product. A discussion of the weights and the effective PIA, variance, and reliability factor is given in section 5.

In the spatial (along-track) surface reference data set, the mean and standard deviation of the NRCS are calculated over a running window of N_s fields of view before rain is encountered (currently, $N_s = 8$). These operations are performed separately for each of the 49 incidence angles for the Ku-band data, corresponding to the cross-track scan from $-18°$ to $+18°$ with respect to nadir. The Ka and KaHS channels are treated in the same way. For the Ka- and DPR channels 25 and 24 angle bins, respectively, are used. For the differential channel, the same procedure is used except that the reference data are formed from the σ^0_{NR}(Ku) $- \sigma^0_{NR}$(Ka) data; in this case, the reference data are computed for the 25 angle bins of the inner swath.

Basic Processing

When rain is encountered, at incidence angle θ_i, the means and standard deviations of the reference σ^0 values are retrieved from the along-track spatial (forward or backward), the hybrid (forward or backward) and the temporal surface reference data sets. If a valid surface reference data set exists for one of the above estimates, then, denoting this by the jth estimate, the 2-way path attenuation (PIA) is computed from the equation:

$$\text{PIA}_j(\theta_i) = \langle \sigma^0_{NR}(\theta_i) \rangle_j - \sigma^0(\theta_i)$$

where $\langle \sigma^0_{NR}(\theta_i) \rangle$ is the mean of the jth rain-free reference estimate and $\sigma^0(\theta_i)$ is the value of the apparent normalized radar surface cross section at the raining field of view of interest.

To obtain information as to the reliability of the jth PIA estimate we consider the ratio of the PIA, as derived in the above equation, to the standard deviation associated with the jth rain-free reference data set. Labeling this standard deviation by σ_j, the reliability factor of the jth PIA estimate is defined as:

$$\texttt{reliabFactor}_j = \frac{\text{PIA}_j}{\sigma_j}$$

which is equal to the inverse of the coefficient of variation of the estimate.

The effective PIA, PIA_{eff}, and the corresponding reliability factor, Rel_{eff}, can be expressed in similar ways. From section 5, we have:

$$\text{PIA}_{\text{eff}} = \frac{\sum u_j \text{PIA}_j}{\sum u_j}$$

$$\text{REL}_{\text{eff}} = \frac{\sum u_j \text{PIA}_j}{\sqrt{\sum u_j}}$$

Where u_j is the inverse of the variance, σ_j^2, associated with the jth reference data set:

$$u_j = \frac{1}{\sigma_j^2}$$

Note that the summations are assumed to range over all valid reference data sets, even if the PIA's are negative. Over land, there can be a maximum of 4 valid reference data sets (forward and backward along-track and two temporal files) while over ocean there can be as many as six since the forward/backward cross-track reference data sets are defined over ocean but not land.

A generalized form of the above equations can be defined, where the various quantities are replaced by the difference between the Ka and Ku-band σ^0 values. Letting $\delta X = X(\text{Ka}) - X(\text{Ku})$, then for the differential PIA, the above equation becomes

$$\delta\text{PIA}_j(\theta_i) = \langle \delta\sigma^0_{NR}(\theta_i) \rangle_j - \delta\sigma^0(\theta_i)$$

The individual and effective dual-frequency estimates at Ku- and Ka-band are then derived from δPIA_j from

$$\text{PIA}_j(\text{Ku}, \theta_i) = \frac{\delta\text{PIA}_j(\theta_i)}{p - 1}$$

$$\text{PIA}_j(\text{Ka}, \theta_i) = \frac{p\,\delta\text{PIA}_j(\theta_i)}{p - 1}$$

where p is the ratio of the path attenuation at Ka-band to that at Ku-band and is nominally set to 6.

3.7.2. Input Variables

sigmaZeroMeasured [real*4]: Normalized backscattering radar cross section of the surface (dB) (NRCS) at Ku-band, Ka-band or KaHS for the angle bins in the radar scan (unitless), from the Preparation Module.

flagPrecip [integer*2]: rain/no-rain flag from Preparation Module.

localZenithAngle [real*4]: Incidence angle from Preparation Module.

landSurfaceType [integer*2]: surface type from Preparation Module. These are modified so that only 3 surface classes are defined: ocean, land and coast.

lat, lon [real*4]: latitude, longitude of the center of the FOV from Preparation Module.

3.7.3. Output Variables

Five sets of path-integrated attenuation and associated quantities are produced. These consist of: single- and dual-frequency derived Ku-band attenuation, single- and dual-frequency derived Ka-band attenuation and a single-frequency derived KaHS-band attenuation. The single-frequency Ku-band attenuation and associated products are stored in the 49 angle bins (full swath) of the Ku-NS structure. The single-frequency Ka/KaHS products are stored in the Ka-MS/Ka-HS structures and are available for the 25 angle bins of the inner swath/ 24 angle bins of the interleaved swath. The dual-frequency PIA products for Ku- and Ka-band are stored in the DPR-NS and DPR-MS structures, respectively, and are produced for the 25 angle bins comprising the inner swath. (For the DPR-NS structure, the dual-frequency derived Ku-band path attenuations are contained in angle bins 13 through 37.) Note that the single-frequency Ku-band results are used in the outer swath of the DPR-NS structure, covering the angle bins from 1 to 12 and from 38 to 49.

The output variables for each of these channels are defined below.

pathAtten [real*4]: The estimated effective 2-way path-attenuation in dB where

$$\texttt{pathAten} = 2\int_0^r k(s)\,ds$$

where $k(s)$ is the attenuation coefficient in dB/km where the integral is taken from the storm top to the surface. The path attenuation is often designated as

the PIA, the path-integrated attenuation. In the notation used above and in section 5:

$$\text{pathAten} = \text{PIA}_{\text{eff}} = \frac{\sum u_j \text{PIA}_j}{\sum u_j}$$

Where u_j is equal to the inverse of the variance associated with the jth reference data point:

$$u_j = 1/\sigma_j^2$$

PIAalt(6) [real*4]: The path-integrated attenuation from the jth estimate, (PIA_j in the notation above), where

PIAalt (1)= PIA derived from the forward along-track spatial reference data

PIAalt (2)= PIA derived from the backward along-track spatial reference data

PIAalt (3)= PIA derived from the forward hybrid/cross-track reference data

PIAalt (4)= PIA derived from the forward hybrid/cross-track reference data

PIAalt (5)= PIA derived from standard temporal reference data

PIAalt (6)= PIA derived from the light-rain temporal reference data

Note that for product versions 1 through 3, the temporal path-attenuation estimate, PIAalt(5), is set to missing but is defined for versions 4 and higher. For product versions 1 through 5, the light-rain temporal estimate, PIAalt(6), is set to missing. Note also that the forward/backward hybrid/cross-track path attenuations are defined only over ocean and are set to missing over land.

PIAweight(6) [real*4]: The weights, w, of the individual PIA estimates used in deriving the effective PIA. The weight for a particular PIA estimate is proportional to the inverse of the error variance associated with the method. The sum of the weights should equal one. As with PIAalt(6), PIAweight(6) is set to missing.

$$w_j = \frac{1}{\sigma_j^2} \frac{1}{\sum \frac{1}{\sigma_j^2}} \equiv \frac{u_j}{\sum u_j}$$

where

$$u_j = 1/\sigma_j^2$$

$$\sum w_i = 1$$

reliabFlag [integer*2]: Reliability Flag for the PIA_{eff} estimate,

$= 1$ if $\text{Rel}_{\text{eff}} > 3$; PIA_{eff} estimate is considered reliable

$= 2$ if $3 \geq \text{Rel}_{\text{eff}} > 1$; PIA_{eff} estimate is considered marginally reliable

$= 3$ if $\text{Rel}_{\text{eff}} \leq 1$; PIA_{eff} is unreliable

$= 4$ if $\text{SNR}_{\text{at surface}} < 2$ dB; provides a lower bound to the path-attenuation

$= 9$ (no-rain case)

reliabFactor [real*4]: Reliability Factor for the effective PIA estimate, pathAtten. This is defined as:

$$\texttt{reliabFact} = \text{Rel}_{\text{eff}} = \left(\sum u_j\right)^{-1/2} \sum u_j \text{PIA}_j$$

RFactorAlt(6) [real*4]: The reliability factors associated with the individual PIA estimates in PIAalt. As with PIAalt(6), RFactorAlt(6) is set to missing.

$$\texttt{RFactorAlt}_j = \text{Rel}_j = \text{PIA}_j/\sigma_j; \qquad j = 1, \ldots, 6$$

refScanID(2,2) [integer*2]: refScanID gives the number of scan lines between the current scan and the beginning (or end) of the along-track reference data at each angle bin. The values are computed by the equation: Current Scan Number − Reference Scan Number. The values are positive for the Forward estimates and negative for the Backward estimates. The Fortran indices are:

> 1,1 - Forward - Near reference
> 2,1 - Forward - Far reference
> 1,2 - Backward - Near reference
> 2,2 - Backward - Far reference

RMS [real*4]: RMS is a weighted version of the root mean square error and provides a measure of the error of the individual PIA estimates from the effective PIA estimate. [Note that this variable is not in the present structure definitions but can be derived from the output variables.]

3.7.4. Temporal Reference Files

Temporal reference files or look-up tables (LUT) are needed to estimate the path attenuation using temporal reference data. The temporal reference data are simply the mean and standard deviations of previously measured rain-free σ^0 data that have been categorized with respect to incidence angle and location. In particular, the LUTs contain the rain-free sample mean and standard deviation of the σ^0 data at each (lat, lon, incidence angle) bin, where the incidence angles, with respect to the radar, consist of nadir, ± 0.710, ± 1.420, $\cdots$ up to the maximum angle. Also stored is the number of σ^0 data points acquired at the particular bin in question and used in computing the statistics.

For version 5 of the algorithm, a 0.50×0.50 grid is used which covers the GPM-DPR latitude range of 67°S–67°N so that 268 latitude bins and 720 longitude bins are needed. Four LUTs are derived from DJF (December-January-February), MAM, JJA, SON input data. For each of these, 5 LUTs are prepared corresponding to ocean, land, coast, sea-ice and snow-covered land backgrounds. Note that separate tables are produced for $\sigma^0(\text{Ku})$, $\sigma^0(\text{Ka})$, $\sigma^0(\text{KaHS})$, and the

difference field, $[\sigma^0(\text{Ka}) - \sigma^0(\text{Ku})]$ so that a total of 20 LUT's are generated for each three-month season.

As noted earlier, two types of temporal reference files have been defined: the standard temporal reference files as described above and a light-rain reference file which, as of version 4 of the code, is undefined. The results derived from the standard temporal reference file can be found in the fifth entry in the variables `PIAalt`, `PIAweight`, `RFactorAlt`. The sixth entry for these variables, corresponding to the 'light-rain' temporal reference file, is set to missing.

3.7.5. Definitions of the Effective PIA, Variance and Reliability Factor

As noted above, multiple estimates of PIA can be generated for each channel corresponding to different surface reference estimates. Specifically, we have the following situation

$$\text{PIA}_j = \langle \sigma^0_{NR} \rangle_j - \sigma^0 \tag{3.7-1}$$

where the first term on the right-hand side is the jth surface reference value and the second term is the apparent NRCS in rain. Associated with the jth reference data set is a variance, σ_j^2:

$$\text{var}(\text{PIA}_j) = \text{var}[\langle (\sigma^0_{NR}) \rangle_j] = \sigma_j^2 \tag{3.7-2}$$

From these PIA estimates we want to obtain an effective or 'best' PIA. We assume it can be written in the form:

$$\text{PIA}_{\text{eff}} = \sum w_j \text{PIA}_j \tag{3.7-3}$$

Where the weights, w_j, are such that

$$\sum w_j = 1 \tag{3.7-4}$$

We assume that the individual PIA estimates are statistically independent so that the variance of PIA_{eff} is:

$$\text{var}(\text{PIA}_{\text{eff}}) = \sum w_j^2 \sigma_j^2 \tag{3.7-5}$$

To minimize this, subject to the side condition given by (3.7-4), we use the method of Lagrange multipliers where the expression

$$\sum w_j^2 \sigma_j^2 + \lambda(\sum w_j - 1) \tag{3.7-6}$$

is minimized with respect to the weights, w_j. Taking the partial derivatives of (3.7-6) with respect to w_i, then

$$2w_i\sigma_i^2 + \lambda = 0 \quad \Rightarrow \quad w_i = -\lambda/2\sigma_i^2 \tag{3.7-7}$$

Also, using (3.7-4) gives

$$\sum w_j = -(\lambda/2)\sum(1/\sigma_j^2) \quad \Rightarrow \lambda = -2/\sum(1/\sigma_j^2) \tag{3.7-8}$$

Substituting (3.7-8) into (3.7-7) gives an expression for the weights:

$$w_j = \frac{1}{\sigma_j^2} \frac{1}{\sum \frac{1}{\sigma_j^2}} \equiv u_j / \sum u_j \qquad (3.7\text{-}9)$$

Where

$$u_j = 1/\sigma_j^2 \qquad (3.7\text{-}10)$$

The effective PIA is then

$$\text{PIA}_{\text{eff}} = \left(\sum u_j\right)^{-1} \sum u_j \text{PIA}_j \qquad (3.7\text{-}11)$$

If we define the reliability factor, Rel, as the ratio of the PIA to the standard deviation of the reference estimate, then for the jth reference estimate, we can write:

$$\text{Rel}_j = \text{PIA}_j / \sigma_j \qquad (3.7\text{-}12)$$

To apply this definition to the present situation, we define Rel_{eff} by the equation:

$$\text{PIA}_{\text{eff}} = \left(\sum u_j\right)^{-1} \sum u_j \text{PIA}_j \equiv \sigma_{\text{eff}} \text{Rel}_{\text{eff}} \qquad (3.7\text{-}13)$$

Computing Rel_{eff} requires a value for the standard deviation of the effective PIA. This can be found by substituting (3.7-9) into (3.7-5) and by noting that $\sigma_{\text{eff}}^2 = \text{var}(\text{PIA}_{\text{eff}})$. This gives

$$1/\sigma_{\text{eff}}^2 = \sum(1/\sigma_j^2) \quad \Rightarrow \quad \sigma_{\text{eff}}^2 = \left[\sum(1/\sigma_j^2)\right]^{-1} = \left(\sum u_j\right)^{-1} \qquad (3.7\text{-}14)$$

Using (3.7-14) in (3.7-13) gives

$$\text{Rel}_{\text{eff}} = \left(\sum u_j\right)^{-1/2} \sum u_j \text{PIA}_j \qquad (3.7\text{-}15)$$

Equations (3.7-9), (3.7-11) and (3.7-15) define, respectively, the weights, effective PIA, and effective reliability factor that are computed in the algorithm. In addition to the σ_{eff} error defined above in (3.7-14), a kind of RMS error can be defined by the following equation:

$$\text{RMS}_{\text{eff}}^2 = \sum_j w_j [\text{PIA}_{\text{eff}} - \text{PIA}]^2 \qquad (3.7\text{-}16)$$

where the summation runs over the j estimates of PIA. Note that when the weighting factors are all the same then this reduces to the usual definition of RMS error.

There are several issues related to these equations. For example, what should be done if none of the reference data sets exist? This situation can occur for measurements over small islands or small bodies of water or at coastal fields of view. For example, over a small island, there may be an insufficient number of non-raining fields of view adjacent to the rain area to form a valid spatial reference. In most cases, the temporal reference data set would be used

and the other reference estimates would be discarded. However, in some cases, there may be an insufficient number of data points in the temporal file to provide a valid estimate. In this case, a flag is set indicating that no valid reference data are available and all the output variables are set to -9999.9

A somewhat different situation occurs if some of the reference data sets exist but all yield a negative PIA. For these cases, the individual variances will exist so that $\mathrm{Rel}_{\mathrm{eff}}$, $\mathrm{PIA}_{\mathrm{eff}}$ and the effective variance should all exist. Note that for these cases $\mathrm{Rel}_{\mathrm{eff}}$, $\mathrm{PIA}_{\mathrm{eff}}$ will be negative but the effective variance will be positive, as it should be.

A third type of situation occurs if one or more of the PIA estimates are positive and one or more of the PIA estimates are negative. In this case, the negative PIAs will be included in the definition of $\mathrm{PIA}_{\mathrm{eff}}$. In general, as long as the reference data is considered to be valid, the PIA will be used even if the value is negative.

According to these scenarios, there will be only one type of raining situation where the output variables will need to be set to some default value and this occurs when none of the reference data sets exist or are valid. This is expected to be a small fraction relative to the total number of rain cases.

3.7.6. Excluding Spatial Reference Data based on the `refScanID` Variable

This section relates to determining the circumstances under which we assume a spatial reference estimate to be valid. For the forward-going spatial reference, reference data will almost always exist. An exception is if rain is encountered at the beginning of the orbit before $N_s(=8)$ rain-free fields of view have been measured at a particular incidence angle. A similar exception occurs for the backward spatial methods: this occurs, however, at the end of the orbit rather than the beginning. In all other cases, forward and backward spatial reference data should exist. The question is how should we exclude spatial reference estimates if the data are taken at locations far from the raining area. To make this definite we implement the following rules in the algorithm.

See definition of `refScanID`(2,2) in section 3.7.3.

The forward along-track spatial reference at angle bin j will be assumed to be invalid if:

$$|\mathtt{refScanID}(2,1,j)| > 50.$$

Similarly, the backward along-track spatial reference at angle bin j will be assumed to be invalid if:

$$|\mathtt{refScanID}(2,2,j)| > 50.$$

The above conditions are equivalent to stating that, for a particular incidence angle, all the spatial reference data must be taken within 50 scans of the scan at which rain is encountered. The criteria for the hybrid cross-track are more complicated because two quadratic fits are used

for the inner and outer portion of the swath. Nominally, we will assume that if there are 15 or more angle bins in the inner portion of the swath for which:

$$|\texttt{refScanID}(2,1,j)| \leq 50$$

then the forward hybrid cross-track method will be applied. Similarly in the outer portion of the swath, if there are 15 or more angle bins in this portion of the swath for which:

$$|\texttt{refScanID}(2,1,j)| \leq 50$$

then the forward hybrid cross-track method will be applied. Application of the backward hybrid cross-track will follow the same rule, based on $\texttt{refScanID}(2,2,j)$.

3.7.7. Additional Comments and Version-dependent Variables

In version 5, sea-ice and snow-covered land surface data from NOAA are now output by the preparation module in the variable $\texttt{snowIceCover}$. The preparation module also outputs $\texttt{landSurfaceType}$, the leading digit of which is used to determine whether the surface is ocean, land or coast. When the $\texttt{snowIceCover}$ variable registers 'sea-ice' and $\texttt{landSurfaceType}$ is 'ocean', then the surface type for the SRT is set to 'sea-ice' and the temporal and spatial reference data for 'sea-ice' are used. Similarly, when the $\texttt{snowIceCover}$ variable indicates snow-cover and $\texttt{landSurfaceType}$ is 'land', then the surface type for the SRT is set to 'snow-cover' and the relevant temporal and spatial reference data are used. On the other hand, if $\texttt{snowIceCover}$ is set to 'sea-ice' and 'landSurfaceType' is not 'ocean' then $\texttt{landSurfaceType}$ is used to identify the surface type. The $\texttt{landSurfaceType}$ variable is also used to override the $\texttt{snowIceCover}$ variable if the later indicates 'snow-cover' but $\texttt{landSurfaceType}$ is not set to 'land'.

Version 5 of the DPR algorithm also produces saturation flags for the surface returns. These flags are generated by the preparation module and given the name $\texttt{flagSigmaZeroSaturation}$. A second set of temporal look-up tables has been prepared so that the 'saturation-corrected' sigma-zero values are not included in the calculation of the statistics. A decision has been made to use the tables that include the 'saturation-corrected' data. As saturation conditions primarily affect the nadir/near-nadir Ku-band data under rain-free conditions, inclusion of the 'saturation-corrected' data will tend to increase the magnitude of the reference data thereby increasing the estimated Ku-band path attenuation. The 'saturation-corrected' $\sigma^0(\text{Ku})$ data will also tend to decrease the dual-frequency estimates of path attenuation because this is computed as the difference between the Ka- and Ku-band path attenuations and, in nearly all cases, only the Ku-band data are affected by saturation.

Because the Ku-band has greater sensitivity than the matched-swath Ka-band, there are a number of cases for which rain is detected at Ku-band but not at Ka-band. As dual-frequency derived estimates at Ku- and Ka-band are produced when either or both channels detect rain,

a number of dual-frequency derived Ka-band estimates of path attenuation will be produced without corresponding single-frequency estimates.

Versions 1 through 3 of the SRT products do not contain path attenuations based on the temporal reference data. Versions 4 and higher will include such results and which can be found in `PIAalt`(5). The light-rain/wet soil temporal reference data set has yet to be derived so this product will be unavailable up to and including version 5. As a consequence `PIAalt`(6) will be set to 'missing' (-9999.9). As already noted, the hybrid/cross-track reference data are derived only over ocean so that over land, `PIAalt`(3) and `PIAalt`(4) are set to 'missing'.

In version 4 or lower, the algorithm does not check for saturated conditions. This can lead to errors in the path-attenuation estimates.

3.8 Solver module

3.8.1 Objective

The primary objective of the Solver module is to retrieve the drop size distribution and calculate some physical variables.

3.8.2 Algorithm Overview

The solver module employs an R-D_m plane, where the vertical axis is the precipitation rate (R) and the horizontal axis is the mass weighted mean diameter (D_m). Once an R-D_m relation (as $R = \epsilon^r p D_m^q$) is assumed, the retrieval process goes from the top to the bottom range bin. At a "precipitating"range bin, a combination of R and D_m which satisfies both the R-D_m relation and the given Z_f is usually selected. Z_f is the radar reflectivity factor corrected for attenuation caused at the higher range bins but not for attenuation caused at the current range bin. For drawing the contour of Z_f on the R-D_m plane, scattering tables are used. After R and D_m are calculated at all "precipitating"range bins, the path integrated attenuation (PIA) is calculated. When the surface reference technique (SRT) gives a reliable PIA estimate, the calculated PIA and SRT's PIA estimate can be compared.

The R-D_m relation is linked to ϵ, which is originally an adjustment factor for the k-Z_e realtion. The retrieval is done multiple times for different ϵ or different R-D_m relations corresponding ϵ ranging from 0.2 to 5.0. The best ϵ or the best R-D_m relation is selected by checking the likelihood of ϵ and the difference between the calculated PIA and SRT's PIA.

3.8.3 Retrieval processes

The major input data to the Solver module are radar reflectivity factor corrected for attenuation by non-precipitating particles (here it is denoted by Z_m), μ and σ of $\log_{10} \epsilon$, SRT's PIA estimates PIA_SRT, its reliability, precipitation type and the information of "phase". The retrieval algorithm first defines range bins to be processed: It mainly processes the data between the storm top and the actual surface.

From the storm top to the clutter free bottom, Z_m is usually available for the retrieval. By correcting the attenuation caused by higher range bins, Z_m is converted to Z_f. Then, the contour of the given Z_f is drawn on the R-D_m plane by reference to the scattering tables. If there is only one crossing point between the contour of Z_f and the curve for the assumed R-D_m relation, R and D_m can be determined easily. If there are multiple crossing points, a set of R and D_m which has smaller R and D_m, is preferred. Unfortunately if there are no crossing points, the point that is on the curve of R-D_m relation and gives the closest Z_f to the given value is selected. In this case, given Z_f (Z_{f1}) and the finally determined Z_f (Z_{f2}) are different.

In the main-lobe clutter region (below the clutter free bottom), Z_m is not useful for the retrieval. Here, the vertical profile of Z_e is assumed to be constant, or the same value of Z_e

at the clutter free bottom is used in the clutter region. The same method is also applied for range bins in which Z_m's are smaller than the noise level if such small Z_m's are caused by large attenuation due to heavy rain above them. Specifically, if Z_m's above the point in question are reliable at 8 (4 for HS) or more liquid-phase range bins in the same pixel, Z_e is extrapolated.

In the dual-frequency algorithm, the following preference is set.

(1) Z_f of KuPR

(2) Z_f of KaPR

(3) extrapolated Z_e of KuPR

(4) extrapolated Z_e of KaPR

3.8.3-1 Determination of ϵ and use of SRT

Different R-D_m relations are tested by changing ϵ from 0.2 to 5.0. Using the following conditions, the best R-D_m relation is selected. Generally, the three conditions a) to c) are checked for the single-frequency algorithms and the four conditions a) to d) are checked for the dual-frequency algorithm.

a) A priori probability of ϵ; $(\log(\epsilon) - \mu)^2$ is minimized, where μ is given by the DSD database or $\mu = 0$ if DSD database is not applied.

b) The difference of PIA calculated by the retrieval (PIA_SLV) and PIA estimated by SRT (PIA_SRT); $(\text{PIA\_SLV} - \text{PIA\_SRT})^2$ is minimized. When PIA_SRT is saturated, $(\min(\text{PIA\_SLV} - \text{PIA\_SRT}, 0))^2$ is minimized.

c) The difference of Z_{f1} and Z_{f2}; The sum of $(Z_{f1} - Z_{f2})^2$ is minimized.

d) If Z_m of KuPR is used for the retrieval and Z_m of KaPR is normal, estimated DSD should be also agreed with KaPR; $(\max(Z_{f2} \text{ of KaPR} - Z_{f1} \text{ of KaPR}, 0))^2 + (\min(Z_{f2} \text{ of KaPR} - Z_m \text{ of KaPR}, 0))^2$ should be minimized. If Z_{f2} of KaPR is between Z_m of KaPR and Z_{f1} of KaPR, the vaule is zero.

The following preference is set to select the use of PIA.

(1) δPIA_SRT=KaPR's PIA_SRT$-$KuPR's PIA_SRT (if both are reliable and not saturated)

(2) KaPR's PIA_SRT (if it is reliable and not saturated)

(3) KuPR's PIA_SRT (if it is reliable and not saturated)

(4) KaPR's PIA_SRT (if it is reliable and saturated)

(5) KuPR's PIA_SRT (if it is reliable and saturated)

If none of PIA_SRT is available, or if selected PIA_SRT is saturated, abnormally high precipitation rates may be resulted. To avoid them, condition e) is used.

e) R estimated from Z_m (not extrapolated Z_e) at liquid-phase range bins should be vertically constant; the variance of R is minimized.

3.8.3-2 NUBF correction

Two NUBF parameters (`p_area` and `rainvar`) are set in the algorithm, but `p_area` (the ratio of rain part in an FOV) is fixed to 1.0 for the version 04 and version 05. `rainvar` (the square of coefficient of variation of R) is estimated by a fractal approach. In the single-frequency algorithms, NUBF correction is not applied in the first main loop. In the second (final) main loop, the NUBF parameter is estimated from `piaFinal` of the first main loop. In the dual-frequency algorithm, the NUBF parameter is estimated from `piaFinal` of the single-frequency algorithms. KuPR's `piaFinal` is preferred to KaPR's `piaFinal`.

4. INTERFACE TO OTHER ALGORITHMS

The combined DPR-GMI algorithm requires outputs from the preparation module (PRE), the vertical profile module (VER), the surface reference technique module (SRT), and the classification module (CSF), in addition to the DPR radar reflectivity profiles. Precipitation detection from the PRE, pressure, temperature and humidity profiles from the VER, the PIA from the SRT, and bright band detection, altitude of the bright band (if it exists), and classification as convective or stratiform precipitation from the CSF will be used in the DPR-GMI combined algorithm.

The DPR products will be utilized also in the GPM Passive Microwave-Radar Enhanced Algorithm of an Optimal Estimation approach that uses the DPR/GMI data as the a-priori constraint.

5. REFERENCES

Awaka, J., T. Iguchi, H. Kumagai, and K. Okamoto, 1997: Rain type classification algorithm for TRMM precipitation radar, *Proc. IEEE IGARSS*, 317–319.

Awaka, J., T. Iguchi, and K. Okamoto, 1998: Early results on rain type classification by the Tropical Rainfall Measuring Mission (TRMM) precipitation radar, *Proc. 8th URSI Commission F Open Symp.*, Aveiro, Portugal, 143–146.

Awaka, J., T. Iguchi, and K. Okamoto, 2009: TRMM PR standard algorithm 2A23 and its performance on bright band detection, *J. Meteor. Soc. Japan*, **87A**, 31–52.

Baldini, L. and E. Gorgucci, 2006: Identification of the melting layer through dual-polarization radar measurements at vertical incidence, *J. Atmos. Ocean. Technol.*, **23**, 829–839.

Bandera, J., A. D. Papatsoris, P. A. Watson, and J. W. Goddard, 1998: Method for detecting the extent of the melting layer, *Electron. Lett.*, **34(22)**, 2104–2105.

Caylor I.J., G.M. Heymsfield, R. Meneghini, and L.S. Miller, 1997: Correction of sampling errors in ocean surface cross-sectional estimates from nadir-looking weather radar. *J. Atmos. Oceanic Technol.*, **14**, 203–210.

Durden, S.L., L. Li, E. Im and S.H. Yueh, 2003: A surface reference technique for airborne Doppler radar measurements in hurricanes, *J. Atmos. Oceanic Technol.*, **20**, 269–275, 2003.

Durden, S.L., S. Tanelli, and G. Dobrowalski, 2010: CloudSat W-band radar measurements of surface backscatter, *IEEE Geosci. Remote Sens. Lett.*, **7**, 401–405, doi: 10.1109/LGRS.2010.2079314.

Durden S.L., S. Tanelli, and R. Meneghini, 2012: Using surface classification to improve surface reference technique over land, *Indian J. Radio & Space Physics*, **41**, 403–410.

Fabry, F. and I. Zawadzki, 1995, Long-term radar observations of the melting layer of precipitation and their interpretation, *J. Atmos. Sci.*, **52**, 838–851.

Hines, E. L., 1983: Image processing techniques for the detection of the radar bright band, Ph.D. dissertation, Univ. Bradford, Bradford, U.K.

Iguchi, T. and R. Meneghini, 1994: Intercomparisons of single-frequency methods for retrieving a vertical rain profile from airborne or spaceborne radar data. *J. Atmos. Oceanic Technol.*, **11**, 1507–1516.

Iguchi, T., T. Kozu, J. Kwiatkowski, R. Meneghini, J. Awaka, and K. Okamoto, 2009: Uncertainties in the Rain Profiling Algorithm for the TRMM Precipitation Radar. *J. Meteor. Soc. Japan, Vol.*, **87A**, 1–30.

Iguchi, T., S. Seto, et al., 2012: An overview of the precipitation retrieval algorithm for the Dual-frequency Precipitation Radar (DPR) on the Global Precipitation Measurement (GPM) missionfs core satellite. *SPIE*, Kyoto, Japan.

Klaassen, W., 1988: Radar observations and simulation of the melting layer of precipitation, *J. Atmospheric Sciences*, **45**, 3741–3753.

Kozu, T., 1995: A generalized surface echo radar equation for down-looking pencil beam radar. *IEICE Trans. Commun.*, **E78-B**, 1245–1248.

Kubota, T., T.Iguchi, M. Kojima, L. Liao, T Masaki, H. Hanado, R. Meneghini, R. Oki, 2016: A statistical method for reducing sidelobe clutter for the Ku-band precipitation radar onboard the GPM Core Observatory, *J. Atmos. Oceanic Technol.*, **33 (7)**, 1413-1428.

Kubota, T., M. Satoh, T. Nasuno, S. Seto, T. Iguchi, R. Oki , 2012: Development of cloud liquid water database using global cloud-system resolving model for GPM/DPR algorithm. *Proc. IGARSS 2012*, 350–353.

Kubota, T., N. Yoshida, S. Urita, T. Iguchi, S. Seto, R. Meneghini, J. Awaka, Member, H. Hanado, S. Kida, and R. Oki, 2014: Evaluation of precipitation estimates by at-launch codes of GPM/DPR algorithms using synthetic data from TRMM/PR observations. *IEEE J. Sel. Topics Appl. Earth Observ. Remote Sens.*, **7**, 3931–3944. (doi.10.1109/JSTARS.2014.2320960.)

Le, M. and V. Chandrasekar, 2013a: Precipitation Type Classification Method for Dual-Frequency Precipitation Radar (DPR) Onboard the GPM, *IEEE Trans. Geosci. Remote Sens.*, **51(3)**, 1784–1790.

Le, M. and V. Chandrasekar, 2013b: Hydrometeor Profile Characterization Method for Dual-Frequency Precipitation Radar Onboard the GPM, *IEEE Trans. Geosci. Remote Sens.*, **51(6-2)**, 3648–3658.

Li, L., E. Im, L.N. Connor, and P.S. Chang, 2004: Retrieving ocean surface wind speed from the TRMM precipitation radar measurements, *IEEE Trans. Geosci. Remote Sens.*, **42**, 1271–1282.

Marzoug, M. and P. Amayenc, 1994: A class of single- and dual-frequency algorithms for rain rate profiling from a spaceborne radar. Part I: Principle and tests from numerical simulations. *J. Atmos. Oceanic Technol.*, **11**, 1480–1506.

Meneghini, R., and T. Kozu, 1990: *Spaceborne weather radar*. Artech House (Boston/London), Norwood, MA, 197pp.

Meneghini, R. and K. Nakamura, 1990: Range profiling of the rain rate by an airborne weather radar. *Remote Sens. Environ.*, **31**, 193–209.

Meneghini, R., T. Iguchi, T. Kozu, L. Liao, K. Okamoto, J.A. Jones, and J. Kwiatkowski, 2000: Use of the surface reference technique for path attenuation estimates from the TRMM Radar. *J. Appl. Meteor.*, **39**, 2053–2070.

Meneghini, R., J.A. Jones, T. Iguchi, K. Okamoto, and J. Kwiatkowski, 2004: A hybrid surface reference technique and its application to the TRMM Precipitation Radar, *J. Atmos. Oceanic Technol.*, **21**, 1645–1658.

Meneghini, R. and J.A. Jones, 2011: Standard deviation of spatially-averaged surface cross section data from the TRMM Precipitation Radar, *IEEE Geosc. Remote Sens. Letters*, **8**, 293–297.

Meneghini, R., L. Liao, S. Tanelli, and S. L. Durden, 2012: Assessment of the Performance of a Dual-Frequency Surface Reference Technique Over Ocean. *IEEE Trans. Geosci. Remote Sens.*, **50**, 2968–2977.

Meneghini, R., and L. Liao, 2013: Modified Hitschfeld-Bordan equations for attenuation-corrected rain reflectivity: Application to nonuniform beamfilling at off-nadir incidence. *J. Atmos. Oceanic Technol.*, **30**, 1149–1160.

Meneghini, R., and H. Kim, 2016: Minimizing the Standard Deviation of Spatially Averaged Surface Cross-Sectional Data From the Dual-Frequency Precipitation Radar. *IEEE Trans. Geosci. Remote Sens.*.

Onogi, K., J. Tsutsui, H. Koide, M. Sakamoto, S. Kobayashi, H. Hatsushika, T. Matsumoto, N. Yamazaki, H. Kamahori, K. Takahashi, S. Kadokura, K. Wada, K. Kato, R. Oyama, T.

Ose, N. Mannoji and R. Taira , 2007 : The JRA-25 Reanalysis. *J. Meteor. Soc. Japan*, **85**, 369–432.

Press W.H. et al., 1992: *Numerical Recipes in FORTRAN, 2nd Edition.* Cambridge University Press. ISBN 0 521 43064 X.

Rosenkranz, P. W., 1975: Shape of the 5mm oxygen band in the atmosphere. *IEEE Trans. Ant. and Propag.*, AP-23, 498–506.

Seto, S. and T. Iguchi, 2007: Rainfall-induced changes in actual surface backscattering cross sections and effects on rain-rate estimates by spaceborne precipitation radar. *J. Atmos. Oceanic Technol.*, **24**, 1693–1709.

Seto, S., T. Iguchi, 2011: Applicability of the iterative backward retrieval method for the GPM Dual-frequency Precipitation Radar. *IEEE Transactions on Geoscience and Remote Sensing*, **49(6)**, pp.1827–1838.

Seto, S., T. Iguchi, T. Oki, 2013: The basic performance of a precipitation retrieval algorithm for the Global Precipitation Measurement mission's single/dual-frequency radar measurements. *IEEE Transactions on Geoscience and Remote Sensing*, **51(12)**, 5239–5251.

Smyth, T. J., A. J. Illingworth, and A. B. Smith, 1998: Radar estimates of rainfall rates at the ground in bright band and non-bright band events, *Q. J. R. Meteorol. Soc.*, **124(551)**, 2417–2434.

Steiner, M., R.A. Houze, Jr., and S.E. Yuter, 1995: Climatological characterization of three-dimensional storm structure from operational radar and rain gauge data, *J. Appl. Meteor.*, **34**, 1978–2007.

Tagawa, T., 2009: Derivation of sub-footprint scale σ^0 observed by TRMM Precipitation Radar. *IEEE. Trans. Geosci. Remote Sens.,IGARSS 2008*, IV, 137–140.

Takahashi, N., and T. Iguchi, 2004: Estimation and correction of beam mismatch of the Precipitation Radar after an orbit boost of the Tropical Rainfall Measuring Mission Satellite, *IEEE. Trans. Geosci. Remote Sens.*, **42**, 2362–2369.

Takahashi, N., H. Hanado, and T. Iguchi, 2005: Estimation of path-integrated attenuation and its nonuniformity from TRMM/PR range profile data. *IEEE. Trans. Geosci. Remote Sens.*, **44**, 3276–3283.

Tan, J. and J.W.F. Goddard, 1995: The use of dual-polarisation techniques for bright-band detection with PPI-based radars, *Eng.-Colloq. Radar Meteorol.*, 11/1–11/6.

Tanelli, S., S.L. Durden, and E. Im, 2006: Simultaneous measurements of Ku- and Ka-band sea surface cross sections by an airborne radar. *IEEE. Trans. Geosci. Remote Sens. Letters*, **3**, 359–363.

Tanelli, S., G.F. Sacco, S.L. Durden, and Z.S. Haddad, 2012: Impact of non-uniform beam filling on spaceborne cloud and precipitation radar retrieval algorithms. *SPIE*, Kyoto, Japan.

Tilford, K.A., I. D. Cluckie, R. J. Griffith, and A. Lane, 2001: Vertical reflectivity characteristics and bright band correction, Proc. Radar Hydrol. Real Time Flood Forecast., *Proc. Adv. Course*, 47–65, European Communities.

Ulaby, F.T., R. K. Moore, and A. K. Fung, 1981: *Microwave Remote Sensing: Active and Passive.* Vol. I. Artech House, Norwood, MA, 456pp.

Waters, J.W., 1976: Absorption and emission of microwave radiation by atmospheric gases, in Methods of Experimental Physics, M. L. Meeks, ed. 12, Part B, *Radio Astronomy*,

Academic Press, Section 2.3.

Yuter, S. E., and R. A. Houze, Jr., 1997: Measurements of Raindrop Size Distributions over the Pacific Warm Pool and Implications for Z-R Relations, *J. Appl. Meteorol.*, **36(7)**, 847–867.

Zrnic, D.S., R. Raghavan, and V. Chandrasekar, 1994: Observations of copolar correlation coefficient through a bright band at vertical incidence, *J. Appl. Meteorol.*, **33(1)**, 45–52.

6. ACRONYMS

BB:	Bright band
CSF module:	Classification module
DB:	dual-beam
DF:	dual-frequency
DFRm:	Measured Dual Frequency Ratio
DPR:	Dual-frequency Precipitation Radar
DSD:	drop size distribution
HS:	high-sensitivity
KuPR:	Ku-band precipitation radar
KaPR:	Ka-band precipitation radar
ML:	Melting layer
MS:	matched scan
NP-attenuation:	Attenuation due to non-precipitation particles
NS:	normal scan
NUBF:	non-uniform beam filling
PIA:	path-integrated attenuation
PRE module:	Preparation module
PSD:	particle size distribution
SB:	single-beam
SF:	single-frequency
SLV module:	Solver module
SRT:	surface reference technique
VER module:	Vertical module